EFFECT OF ADHESIVE STIFFNESS AND CFRP GEOMETRY ON THE BEHAVIOR OF EXTERNALLY BONDED CFRP RETROFIT MEASURES SUBJECT TO FATIGUE LOADS

by

Andrew Viccaro Zorn

Bachelor of Science in Civil Engineering, University of Pittsburgh, 2004

Submitted to the Graduate Faculty of

the School of Engineering in partial fulfillment

of the requirements for the degree of

Master of Science

University of Pittsburgh

2006

UNIVERSITY OF PITTSBURGH

SCHOOL OF ENGINEERING

This thesis was presented

by

Andrew Viccaro Zorn

It was defended on

March 8, 2006

and approved by

Dr. Christopher J. Earls, Chairman and Associate Professor,
Department of Civil and Environmental Engineering

Dr. Amir Koubaa, Academic Coordinator and Lecturer,
Department of Civil and Environmental Engineering

Dr. Kent A. Harries, Assistant Professor,
Department of Civil and Environmental Engineering
Thesis Advisor

EFFECT OF ADHESIVE STIFFNESS AND CFRP GEOMETRY ON THE BEHAVIOR OF EXTERNALLY BONDED CFRP RETROFIT MEASURES SUBJECT TO FATIGUE LOADS

Andrew Viccaro Zorn, MS

University of Pittsburgh, 2006

Nine 10” (254 mm) deep, 6” (152 mm) wide and 186” (4730 mm) long concrete beams having three #4 longitudinal steel reinforcing bars as primary flexural reinforcement, were tested under midpoint cyclic loading until fatigue-induced failure or to 2,000,000 cycles. Eight beams were strengthened with four different soffit-mounted externally bonded carbon fiber reinforced polymer (CFRP) arrangements. A commercially available 4” (102 mm) wide, 0.055” (1.4 mm) thick preformed unidirectional carbon fiber reinforced strip system was used along with two commercially available adhesive systems. The adhesive systems consisted of a high-modulus and a low-modulus adhesive with their respective stiffness’s varying by a factor of two. The effects of CFRP geometry, the width of the strip to the width of the soffit of the beam ratio (b_f/b), and adhesive shear stiffness on the behavior of fatigue loaded specimens were investigated.

Four of the retrofit specimens failed due to fatigue-induced internal reinforcement rupture prior to achieving 2,000,000 cycles. Observations of these specimens include stress range drift from cycle N=2 and N=N_f, degradation of secant stiffness, and the effects of retrofit geometry on the stress carried by the steel reinforcement. Stresses at cycle N=N_f were noted to increase significantly from cycle N=2. The CFRP was noted to increase the secant stiffness of the retrofit specimens and slow the rate of decay of stiffness when compared to the control fatigue specimen. As CFRP area increased, the stress in the steel reinforcing was noted to decrease. The

reduction in steel reinforcement stress for the load range in this research is proportional to the amount of CFRP attached to the soffits of the beam.

The other four retrofit specimens were cycled to 2,000,000 cycles and then tested monotonically to failure. Observations of these specimens indicate that the cyclic loading had significant effect on the bond using the low-modulus adhesive. In the companion thesis, Reeve (2005), Reeve states that the low-modulus adhesive consistently exhibited superior debonding behavior to the high-modulus adhesive. This effect is apparently negated by the effect of cyclic loading for the low-modulus adhesive.

TABLE OF CONTENTS

LIST OF TABLES

LIST OF FIGURES

NOMENCLATURE

Abbreviations

ACI	American Concrete Institute
CAA	conventional adhesive applied [FRP system]
CEB	Comité Euro-International du Beton
CFRP	carbon fiber-reinforced polymer
FIRR	fatigue-induced reinforcing steel rupture
FRP	fiber-reinforced polymer
JSCE	Japan Society of Civil Engineers
LVDT	linear variable displacement transducer
NSM	near-surface mounted [FRP system]
RC	reinforced concrete

Notation

a	shear span of beam
A_c	concrete cross-sectional area
A_f	FRP cross-sectional area
A_s	steel reinforcement cross-sectional area
b	width of RC member (tension face)
b_f	width of FRP strip
E	modulus of elasticity
E_f	FRP modulus of elasticity
E_s	steel modulus of elasticity
f_c	compressive concrete strength
f_c'	28 day concrete compressive strength

f_{fu}	ultimate capacity of FRP
f_{fud}	allowable stress in FRP to mitigate debonding
f_{fuf}	stress limit in FRP under fatigue load conditions
f_u	ultimate strength of steel reinforcement
f_y	yield strength of steel reinforcement
G_a	adhesive shear modulus
$G_a t_a$	adhesive shear stiffness (modulus multiplied by thickness)
G_f	critical fracture energy
h	depth of concrete section
k_b	factor accounting for b_f/b in design
k_{b2}	value of k_b calculated for H2 or L2 (as appropriate)
$k_{bspecimen}$	value of k_b calculated for the specimen considered
k_L	factor accounting for $L_b < L_{bmax}$ in design
L	beam clear span length
L_b	provided anchorage bond length
L_{bmax}	effective anchorage bond length
N	fatigue cycle number
N_f	fatigue failure cycle
n	number of plies of FRP
P	applied load at midspan
S	stress range in reinforcing steel
s	FRP spacing in slab retrofit
t_a	adhesive thickness
t_f	FRP thickness
V_c	shear strength
α	empirical constant

ε_{fu}	*in situ* rupture strain of FRP
ε_{fub}	strain in FRP when debonding occurs
$\varepsilon_{fubspecimen}$	debonding strain for the specimen considered
ε_{fub2}	debonding strain for H2 or L2 (as appropriate)
κ_m	ACI 440.2R strain reduction factor
μ	empirical constant
$\rho_{equivalent}$	equivalent steel ratio
ρ_s	steel reinforcement ratio
σ_f	fatigue stress level in FRP

This dissertation was completed using US units throughout except where noted. The following "hard" conversion factors were used:

1 inch = 25.4 mm

1 kip = 4.448 kN

1 ksi = 6.895 MPa

Reinforcing bar sizes are given using the designation cited in the appropriate reference. In the report, a bar designated with a "#" followed by a number refers to a standard inch-pound designation used in the United States (e.g.: #7). The number refers to the diameter of the bar in eighths of an inch. A bar designated with an "M" after the number refers to the standard metric designation. The number refers to the nominal bar diameter in mm (e.g.: 20M).

1.0 INTRODUCTION AND LITERATURE REVIEW

This chapter presents an introduction to the research presented in this thesis and an extensive literature review.

1.1 INTRODUCTION

The use of fiber-reinforced polymer (FRP) for reinforcing and strengthening concrete elements is a broad topic. There are a number of different applications for using these materials for structural repair and retrofit. The method of application discussed in this work is the so-called Conventional Adhesive Applied (CAA) FRP. This method involves the use of a structural adhesive to bond the FRP material to the soffit of a reinforced concrete member. The CAA method is a "bond critical" (rather than "contact critical") FRP application, indicating that stress transfer between the FRP and substrate concrete is entirely dependent on the bond across the interface of the two materials. As in any reinforced concrete design, monotonic and fatigue loading conditions must be considered. Monotonic loading is the subject of the companion thesis (Reeve, 2005) to the work presented here. The companion work covers the effects of monotonic loading on carbon-fiber reinforced polymer (CFRP) retrofit reinforced concrete beams having the same details and test parameters as those reported here. Thus, the specimens tested by Reeve are the monotonic control specimens for those reported here. The topic of this work is the effect of fatigue loading conditions on CFRP enhanced reinforced concrete beams. This work and the companion work can be applied to the repair and retrofit of reinforced concrete members using CFRP. Some of the procedure and protocol reported here is similar to that reported by Reeve and is repeated here for completeness and clarity.

1.2 OBJECTIVE

The purpose of this thesis is to investigate and gather more information regarding the behavior of fiber-reinforced polymer (FRP) retrofitting subject to fatigue loading conditions. This study focuses on intermediate crack-induced (so called "midspan") debonding of the FRP from the concrete substrate. Concrete cover delamination (or "end-peel") debonding has been effectively mitigated in the reported test specimens by extending the FRP across the entire shear span.

In the United States, ACI 440.2R-02 *Guide for the Design and Construction of Externally Bonded FRP Systems for Strengthening Concrete Structures* is the recognized guideline for the use of FRP retrofitting. Even though it is the presiding document regarding the use of FRPs for repair, ACI 440.2R-02 recommendations with respect to bond behavior are often unconservative when compared to available experimental test data (ACI 440 Bond TG, 2006). To mitigate debonding, ACI 440.2R-02 limits the allowable strain in the FRP based only on FRP material properties without reference to substrate properties. For fatigue applications, a second strain limit is applied which must be satisfied in addition to that to mitigate debonding. As will be discussed, the fatigue limit is not related to bond in the present version of ACI 440.2R-02. Additionally, factors such as the material properties of the adhesive or the strength of the concrete are not included in the recommendations provided by ACI 440.2R-02. Part of the purpose of this research is to support the updating of ACI's recommendations. There are several other code documents that address this issue; they will be discussed in the literature review.

1.3 SCOPE OF REPORT

This thesis presents the experimental study of the fatigue performance of medium scale reinforced concrete beams strengthened with carbon fiber reinforced polymer (CFRP) strips of

varying width applied with adhesives having different properties. The thesis is organized as follows:

- Chapter 1 presents an extensive review of previous related research concerning fatigue performance.
- Chapter 2 presents, in detail, the experimental program devised to evaluate the fatigue performance of the CFRP strengthened reinforced concrete beams. The beam fabrication and CFRP application are also outlined in this section.
- Chapter 3 presents the results of the experimental program.
- Chapter 4 presents a discussion of the results of the experimental program.
- Chapter 5 presents a summary, conclusion, and further research needs.

1.4 LITERATURE REVIEW

The following sections provide an extensive review of available material concerning the fatigue of FRP materials and reinforced concrete beams retrofitted with FRP materials. The companion thesis is also summarized in this section.

1.4.1 Fatigue Performance of FRP Materials

FRP materials are composed of high-performance fibers embedded in a polymeric matrix. The fibers can be carbon, aramid, glass, or a combination of any of these. Not only can FRPs be composed of several different fibers but they also come in a variety of different forms, such as dry woven sheets and tows and preformed shapes including strips and bars. When discussing FRPs, one must recognize that the final or *in situ* properties of the FRP product or structure differ significantly from the properties of individual constituent fibers. Due to the proprietary nature of FRP products and not particularly the fibers, it is always recommended to consult the material data sheets for useable material properties (ACI 440.2R-02). Material properties will vary from

one manufacturer to another. This thesis focuses primarily on the fatigue behavior of unidirectional carbon FRP (CFRP) strips.

Most unidirectional FRP materials exhibit similar fatigue properties. Research unanimously shows that FRP materials exhibit fatigue behavior which far surpasses that of steel (Agarwal and Broutman, 1990; El-Tawil et al., 2001; Barnes and Mays, 1999; Deskovic et al., 1995; Breña et al., 2002). Steel is a crystalline structure and when a defect is present and fatigue loading is applied, the defect initiates a crack; with continued cyclic loading, the crack propagates and eventually a brittle rupture occurs. What characterizes fatigue failure is that the fatigue load to cause failure is below the material's yield strength. FRP strips, on the other hand, are composed of unidirectional fibers aligned in a resin matrix. In general, the fibers used in FRPs have very few defects. Because the fibers have few defects and are embedded in a matrix which is typically considerably weaker than the fibers, FRP materials exhibit considerable resistance to fatigue damage. Damage propagating in the matrix is quickly arrested by the high-strength fibers. Some research shows that fatigue damage is virtually non-existent in FRP materials (Deskovic et al., 1995).

A significant amount of data is available concerning the fatigue behavior of FRP materials themselves (National Research Council, 1991). Generally, this data shows a 5% loss in stress range carrying capacity (S) per decade of logarithmic life (N) for CFRP (Curtis, 1989). Glass FRP (GFRP) and Aramid FRP (AFRP) exhibit a slightly greater rate of degradation; typically about 10% per decade (Mandell, 1982 (GFRP); Roylance and Roylance, 1981 (AFRP)). By comparison, the stress range capacity of mild steel degrades at a rate of about 22% per decade. Representative S-N curves for CFRP, GFRP, and AFRP are shown in Figure 1-1 (Barnes and Mays, 1999) and a representative S-N curve for steel reinforcing bars is shown in Figure 1-2

(Tilly and Moss, 1982). The S-N curve for CFRP (Figure 1-1) is noticeably flatter than the companion S-N curve for steel. This indicates that a long fatigue life (N) can be attained despite the stress range (S) being near the material's ultimate capacity.

Because FRP materials are heterogeneous, their fatigue behavior is complex. Many damage mechanisms exist: matrix cracking, fiber-matrix debonding, delamination, void growth and fiber breakage (Hahn, 1979). The most common damage mechanism is cracking of the matrix. Because of the structure of an FRP, the crack will start in the epoxy matrix and attempt to propagate through the adjacent fibers. The individual fibers have a high toughness and therefore exhibit crack arresting properties. It is these properties that contribute to the good fatigue performance of FRPs. It is assumed that the excellent fatigue behavior exhibited by FRP materials when tested in direct tension in air will also be exhibited when the FRP is used as a flexural retrofit. Therefore fatigue failure of the FRP material itself is not a design issue since the fatigue behavior of the existing reinforcing steel will dominate the fatigue performance. The interface between the FRP and the concrete substrate and the stress level in the steel reinforcing are the limiting factors in design. For the application studied in this research, fatigue of the CFRP itself is not a factor.

1.4.2 Fatigue Behavior of Externally Bonded FRP Reinforcement

This section covers the documented behavior of reinforced concrete members retrofitted with externally bonded FRP reinforcement subject to fatigue loading. The known research studies in this are: Meier et al. (1993), Heffernan (1997), Barnes and Mays (1999), Shahawy and Beitelman (1999), Papakonstantinou et al. (2001), Masoud et al. (2001), Breña et al., (2002), Gussenhoven and Breña (2005), Quattlebaum et al. (2005), and Aidoo et al. (2004 and 2006). Unlike monotonic tests, where FRP properties govern the observed strength increase and

ultimate behavior, the fatigue behavior of flexurally retrofitted concrete beams is controlled by the fatigue behavior of the longitudinal reinforcing steel (Papakonstantinou et al., 2001).

Assuming strain continuity between the concrete, reinforcing steel and the FRP retrofit, one assumes that the FRP relieves some of the transient stress from the reinforcing steel and thus improves the fatigue life of the reinforcing steel and thus the concrete member. Much of the research completed in this area reports reduced reinforcing steel strains and a corresponding increased fatigue life. Two of the reported studies, Heffernan (1997) and Masoud et al. (2001), report an initial reduction in stress in the reinforcing steel but no apparent increase in fatigue life. This observation may be attributed to the initially reduced stress range in the steel reinforcing quickly returning to the stress range corresponding to no FRP retrofit. This behavior suggests strain discontinuity and relative slip or debonding between the FRP and the concrete substrate relieving some of the stress carried by the FRP. To satisfy equilibrium, the reinforcing steel stress must therefore increase. The different observations reported in these studies appear to be related to the nature of the bond between the FRP and the concrete. It is hypothesized that the shear properties – both modulus and bond line thickness – of the adhesive systems used in these studies, may account for the variability of experimental results (Harries, 2005). Despite these differences, the eventual fatigue failure is similar to that of an unretrofit specimen. Behavior is controlled by the fatigue behavior of the reinforcing steel.

Increases in the fatigue life of retrofit specimens can be attributed to the reduced strains carried by the steel. This only holds true if the FRP remains adequately bonded to the substrate. If debonding occurs, the steel stresses, and thus fatigue behavior, return to that of an unretrofit specimen. In most cases, the FRP has apparently remained bonded throughout fatigue loading

histories, although, as discussed below, debonding has been occasionally observed (Quattlebaum et al., 2005) and is suspected to have been present in other studies.

An S-N plot containing all known FRP retrofit research specimens having CAA FRP applications is shown in Figure 1-3. Two existing models of reinforcing bar fatigue behavior, for bars tested in air (Moss, 1980), and bars tested in concrete in a flexural test (CEB, 1990) are also presented in Figure 1-3:

Bars tested in air (Moss, 1980):

$$S^9 N = 3.09x10^{27} \text{ (MPa units)} \qquad (1\text{-}1)$$

Bars tested in concrete (CEB, 1990):

$$S^5 N = 4.0841x10^{17} \text{ (MPa units)} \qquad (1\text{-}2)$$

The CEB (1990) model appears to be reasonable model for design purposes and recognizes the endurance limit at 30 ksi (210 MPa). The Moss (1980) model is included for reference only.

The database from which Figure 1-3 was generated is shown in Table 1-1. The database presents all the current known fatigue tests of reinforced concrete beams retrofit (for flexure) with FRP. Table 1-1 includes all relevant test parameters and failure modes. The research discussed in the following text is included within this database.

Quattlebaum (2003) reports that preformed strip CAA retrofits result in an improved S-N performance over the original unretrofit condition. Debonding was only evident after fatigue failure of a reinforcing bar (effectively failure of the specimen). Debonding, in such cases, results from a) the sudden release of energy associated with the reinforcing bar rupture, and b) the sudden increase in the stress range in the remaining steel and the CFRP. Such failures are typical of the majority of previous research done in this area. Barnes and Mays (1999) and

Shahawy and Beitelman (1999) both report a significant reduction in reinforcing bar stress and a corresponding increase in fatigue life for FRP retrofitted sections. Shahawy and Beitelman also demonstrated that severely damaged beams could be effectively rehabilitated with FRP.

Meier et al. (1993) reports glass/carbon FRP strips bridging cracks resulting from the fatigue failure of the primary reinforcing steel. Tests were continued until the eventual fatigue failure of the FRP strips. These observations are a clear indication of sound bond.

Papakonstantinou et al. (2001) conducted a test program where the stress range in the reinforcing steel was kept constant for both unretrofit and retrofit specimens. This was done by varying the applied load to attain the same stress level. No discernable difference in fatigue life was noted for any of the specimens. This result demonstrated that the FRP does not change the fundamental fatigue performance of retrofit members, although it may increase the fatigue life at a particular load range by reducing the reinforcing steel stress range; however when the stress range in the steel is kept constant, the fatigue failures occur as if the member were unretrofit. Debonding was not observed by Papakonstantinou et al., however the FRP used in these tests was extended over and consequently anchored by the beam supports. This condition is unrealistic and should be expected to improve debonding behavior.

Heffernan (1997) reports an opposite result to Papakonstantinou et al.. Heffernan argues that beams with an FRP retrofit should exhibit enhanced fatigue behavior over identical unretrofit beams even in cases where the steel stress range is held constant. Heffernan states that the concrete softens during cycling and steel stress rises due to the redistribution of the applied stresses. If FRP is present, the FRP will absorb some of the redistributed stresses and thus increase the fatigue life of retrofit specimens. Heffernan further states that when FRP is applied, more frequent smaller cracks form and the localized stress effects on the steel reinforcing are

reduced. This would result in less severe local stress risers in the reinforcing steel and thus an enhancement in fatigue life. Heffernan estimates this increase in fatigue life at 2%. Such a small increase in fatigue life would require an extensive test program, beyond the means of most laboratories, to confirm due to the large expected scatter in fatigue test results. In all cases, Heffernan reports either failure at rupture of the reinforcing steel or rupture of the reinforcing steel followed by CFRP debonding. It is also reported that minimal degradation of the FRP-to-concrete bond was evident. This research also identifies reinforcing steel stresses being the controlling factor in design.

Breña, Wood and Kreger (2002) conducted tests using a wet lay-up CFRP system. Transverse CFRP straps were also used to delay debonding of the CFRP plates. This study reports that when the stress range in the reinforcing is 50% of the yield stress, no debonding or reinforcing bar rupture was noted through 1 million cycles. When the stress range was 90% of the yield stress, both delamination of the CFRP and rebar rupture were the observed failure modes (see Table 1-1).

Three modes of failure for FRP retrofit beams subject to fatigue loading have been identified in previous studies: FRP delamination, FRP fatigue failure, and reinforcing steel rupture. By far, the most common mode of failure is fatigue-induced rupture of the reinforcing steel. The number of cycles to failure when this failure mode controls the fatigue-life of the specimens has not been found to be significantly different from unstrengthened reinforced concrete beams (Harries, 2005). This is evident from the S-N plot showed in Figure 1-3.

1.4.3 State of Practice

This section covers current code documents, guidelines and recommendations put forth by the various governing code writing institutions. These institutions include the American

Concrete Institute (ACI), The Concrete Society (Great Britain), Japan Society of Civil Engineers (JSCE), National Research Council (Italy), and the International Federation for Structural Concrete (CEB - European Union). The recommendations are summarized in the following sections. In addressing fatigue, the ACI and Concrete Society require the designer to verify that the expected FRP stress/strain is lower than an absolute limit associated with the FRP material and not specifically associated with debonding behavior. The JSCE and Italian approaches, on the other hand, provide an additional reduction factor, to be applied to debonding stress/strain limits determined for static loading conditions. The CEB does not quantitatively address fatigue loading. Table 1-2 summarizes the approaches.

1.4.3.1 ACI: ACI440.2R-02

Section 9.5 of ACI 440.2R-02 discusses fatigue stress limits in the CFRP. To mitigate debonding under static loading conditions, ACI 440.2R-02 limits the strain in the FRP to $\kappa_m \varepsilon_{fu}$, where ε_{fu} is the rupture strain of the FRP. Equation 1-3 defines κ_m, as a function of only the FRP stiffness, $nE_f t_f$, where n is the number of layers of FRP and E_f and t_f are the modulus and thickness of a single layer of FRP. In Equation 1-3, a stiffer FRP material results in a lower allowed FRP strain to be developed. Equation 1-3 does not address substrate concrete or adhesive properties.

$$\kappa_m = \begin{cases} \dfrac{1}{60\varepsilon_{fu}}\left(1 - \dfrac{nE_f t_f}{2{,}000{,}000}\right) \le 0.90 \;\; for \;\; nE_f t_f \le 1{,}000{,}000 \text{ lb/in.} \\ \dfrac{1}{60\varepsilon_{fu}}\left(\dfrac{500{,}000}{nE_f t_f}\right) \le 0.90 \;\; for \;\; nE_f t_f > 1{,}000{,}000 \text{ lb/in.} \end{cases} \quad \text{(US units)} \quad (1\text{-}3)$$

$$\kappa_m = \begin{cases} \dfrac{1}{60\varepsilon_{fu}}\left(1-\dfrac{nE_f t_f}{360{,}000}\right) \le 0.90 \;\; for \;\; nE_f t_f \le 180{,}000 \text{ N/mm} \\ \dfrac{1}{60\varepsilon_{fu}}\left(\dfrac{90{,}000}{nE_f t_f}\right) \le 0.90 \;\; for \;\; nE_f t_f > 180{,}000 \text{ N/mm} \end{cases} \quad \text{(SI units)} \qquad (1\text{-}3)$$

Reeve (2005) shows that debonding strains calculated using Equation 1-3 are generally unconservative.

For fatigue loading, maximum allowable stresses in the FRP given in Table 1-2 are applied. These stress limits are reported to be appropriate for creep-rupture and fatigue considerations. For CFRP, the sustained load plus cyclic service load stress limits in the FRP is limited to $0.55f_{fu}$. This value is based on the observed nominal limit of $0.91f_{fu}$ factored by the material resistance factor 0.60 (Similar limits are found for GFRP and AFRP as shown in Table 1-2). Thus the fatigue limit is based only on the excellent fatigue performance of the FRP material itself. Although not explicitly stated, the stress in the reinforcing steel of an FRP-repaired section must also be verified for its fatigue performance. As discussed, this latter limit will typically control fatigue behavior. Additionally, it has been shown (Harries and Aidoo, 2005) that the bond is also affected by fatigue loading. This research focused upon this final point. In any case, the ACI 440.2R-02 limit for fatigue stress in CFRP of $0.55f_{fu}$ is unconservative.

The ACI Committee 440F Task Group on Bond has proposed changes to the ACI 440.2R design philosophy including: imposing stress limits on reinforcing steel, considering FRP and concrete cover delamination separately, reducing the allowable FRP strains in most cases and considering fatigue and creep rupture as separate failure modes having different (and reduced) limits. The Task Group's recommendations are being refined and the data from the present study will contribute to new proposed revisions.

1.4.3.2 The Concrete Society: Technical Report No. 55

Section 6.8.3 of Technical Report No. 55 (Concrete Society, 2004) discusses fatigue of FRP retrofitted members. The Concrete Society states that when a member is subject to fatigue, the typical failure mode is yield of the steel reinforcement followed by debonding of the FRP. Similar to the other code documents, fatigue failure of the reinforcing steel is the primary failure mode. The stress range in the steel due to cyclic loading must to be checked in order to verify that fatigue is not a concern. Similar to ACI 440.2R-02, the Concrete Society also recommends limits on the permissible stress range in the FRP for fatigue applications. These limits are presented in Table 1-2 and are prescribed to control the fatigue behavior of the FRP plate or strip bonding application by limiting the cyclic stresses applied to the FRP material. In a realistic plate bonding application of CFRP, such as this study, a stress range of $0.80f_{fu}$ would be nearly impossible to achieve. Either delamination of the CFRP through the concrete substrate before $0.80f_{fu}$ was attained or reinforcing bar failure followed by CFRP delamination would occur. In the companion work for this study (Reeve, 2005); the maximum stress developed in the CFRP in a monotonic test was approximately 188 ksi (1296 MPa). This is $0.46f_{fu}$ for the material studied. Research shows that $0.80f_{fu}$ is a challenge to attain for surface applied CFRP materials (Reeve, 2005).

1.4.3.3 JSCE: Concrete Engineering Series 41

The Japanese Society of Civil Engineers' recommendations (JSCE, 2001) Section C6.4.11 limit stress in the FRP as a function of FRP properties and interface characteristics. The analysis of the retrofit member is carried out using a sections analysis based on the existing member properties. This means that fatigue in the reinforcing steel is the controlling limit state. JSCE recommends a maximum stress in the FRP to mitigate peeling failures of the FRP. Equation 1-4 serves as a check to ensure that the FRP stress is below a certain level and is secondary to fatigue

rupture of the steel. If the stress in the FRP, σ_f, satisfies Equation 1-4, then a peeling failure will not occur.

$$\sigma_f \le \sqrt{\frac{2\mu G_f E_f}{n t_f}} \qquad \text{(MPa units)} \qquad (1\text{-}4)$$

G_f is the interfacial fracture energy corresponding to debonding of the continuous FRP sheet and concrete (given in units of N/mm). This value can be determined from bond strength tests of FRP materials to concrete. If these tests are not available or data is not available, a value of 0.5 N/mm is permitted to be used. G_f may vary based on the number of plies of FRP, the type of adhesive used, and the strength of the concrete. It is recommended that this value be determined from experiments because it is highly variable and the default value of 0.5 N/mm is suspect. The use of a fracture mechanics approach to design for bond, although perfectly correct, is not believed to be practical for day-to-day design office work and is greatly resisted in North American practice.

In Equation 1-4 is the factor μ. μ is equal to unity for static loading and μ = 0.7 when fatigue loading conditions are expected. Although not explained in the JSCE recommendations, this factor is understood to account for deterioration of bond properties (specifically the fracture energy) under fatigue loads. The effect of accounting for fatigue loads is therefore to reduce the allowable FRP stress to $\sqrt{0.7} = 0.84$ times that permitted under static load conditions.

1.4.3.4 National Research Council (Italy): CNR-DT 200/2004

Like the JSCE recommendations, the Italian National Research Council recommendations (CNR, 2004) prescribe an additional factor, $\eta_1 = 0.5$ which is applied to the allowable FRP debonding stress for cases of cyclic or fatigue loading conditions. This factor is applied in addition to all other factors accounting for environmental exposure, substrate preparation, etc.

Additionally, the stress range in the reinforcing steel is checked to ensure fatigue failure of the steel is not a limit state.

1.4.3.5 International Federation for Structural Concrete: Bulletin 14

Section 9.9 of Bulletin 14 (CEB 2001) identifies fatigue loading as an area where little data is available. No quantitative guidance is provided, although FRP debonding stress limits are prescribed for static load cases. Bulletin 14 restricts the stress range in the reinforcing steel to that present in an unstrengthened beam. This implies that accounting for the FRP reducing the stress in the steel can be used to the design's advantage.

1.4.4 Summary of Companion Thesis, Reeve 2005

The work of Reeve (2005) is presented in this section. Reeve reports the first phase of this two phase research initiative. In Reeve's study, the effects of monotonic loading on CFRP retrofitting were considered. The specimens reported by Reeve will serve as the monotonically loaded companion specimens to those reported here.

1.4.4.1 Debonding Mitigation

Effective debonding mitigation is an important topic when discussing FRP retrofitting. It is very important that the retrofit stays intact throughout the service life of the beam. Through much research, it is concluded that extending the FRP to zero-moment regions effectively mitigates concrete cover delamination (also referred to as end-peel debonding). It can be shown that the peeling stress generated in the FRP is directly related to the distance from the zero-moment region (Sebastian, 2001). Zero-moment regions are considered the support regions in simply supported beams and points of inflection in continuous spans where negative moment regions are present. In this study and Reeve (2005), the CFRP was extended to the supports, effectively mitigating cover delamination. Beyond limiting the interfacial stress, there is no

recognized method of mitigating FRP debonding in the shear span of the beam (referred to as "mid span" or "in-span" debonding).

The use of U-shaped straps to "clamp" the FRP to the soffit of the member over its span has been attempted in order to mitigate debonding. This system has been shown to increase the maximum strain in the FRP by as much as 20%, although the increase in capacity of the member was insignificant (Kotynia and Kaminska, 2003). Contrary to Kotynia and Kaminska (2003), Maeda et al. (2002) suggests that strains in the FRP were not increased by U-wrapping but actually decreased. This is due to the flexible adhesive layer being constrained and no longer being effective. A decrease in deformation of beams with U-wraps was also noted. This further suggests that U-wrapping is an ineffective method of mitigating in-span FRP debonding.

1.4.4.2 Conclusions from Reeve (2005)

Reeve (2005) considered a number of parameters (also considered in this work) and drew the following conclusions relevant to the present work.

The b_f/b ratio is the total CFRP strip width-to-soffit ratio. Reeve considered three different b_f/b ratios: 0.16, 0.33, and 0.66. In order to further investigate this effect, two different strip arrangements, one having a single 2 inch (52 mm) wide strip, and one having two 1 inch (25 mm) wide strips were tested each having $b_f/b = 0.33$. Reeve concluded that the specimen geometry (CFRP arrangement and width) has an effect on the ductility, general yield loads, flexural strength, and the debonding behavior of the material. In general, increased general yield and maximum loads correlated with increasing b_f/b ratios. The more CFRP adhered to the soffit, the stronger the beam was. However, the increase in capacity was not proportional to the area of CFRP indicating a reduced CFRP efficiency with increasing b_f/b ratio (or CFRP area). Ductility also decreased with increased strip width. Reeve also concluded that multiple thinner strips are

preferable to fewer wider strips. An increase in ultimate load and ductility was seen when multiple thinner strips were used.

Two commercially available adhesives, with significantly different moduli, were used to apply the CFRP strips to the concrete substrate (these are described in Chapter 2). This was done to analyze the effects of a stiff and softer adhesive. Higher general yield loads, ultimate capacities, and maximum deflections were seen when using the low-modulus adhesive.

Reeve additionally concluded that the ACI440.2R-02 recommendations for the bond dependant coefficient, κ_m (Equation 1-3, above), were generally unconservative. In his studies, κ_m overestimated the strain where debonding becomes likely by as much as two fold for the stiff adhesive and less so for the softer adhesive. This demonstrates that ultimately the nature of the adhesive should be included when determining limiting debonding strains.

In a comparison of existing models for debonding behavior, Reeve concluded that the model proposed by Teng et al. (2004) best predicted the observed data:

$$\varepsilon_{fub} = \alpha k_b \sqrt{\frac{\sqrt{f_c'}}{nE_f t_f}} \quad \text{(SI Units)} \tag{1-5}$$

$$\text{where } k_b = \sqrt{2 - \frac{b_f}{b} \Big/ 1 + \frac{b_f}{b}} \tag{1-6}$$

The α term in Equation 1-5 is an empirical constant dependent on loading and member geometry. Teng et al. (2001) recommend a value of $\alpha = 1.1$. Reeve recommends that this constant may be calibrated to include the effect of adhesive properties.

1.4.4.3 ACI Task Group on Bond (2006)

In a similar recent reliability analysis of available data conducted by the ACI Task Group on Bond, the following relationship was shown to provide the best correlation with available test results of FRP retrofit concrete beams experiencing debonding failures:

$$\varepsilon_{fub} = 0.42\sqrt{\frac{f_c'}{nE_f t_f}} \qquad \text{(SI Units)} \qquad (1\text{-}7)$$

No previous studies have documented appropriate adjustments for fatigue loading conditions.

Table 1-1 Summary of available fatigue data from FRP-strengthened concrete beams.

Researcher	Specimen	b (in)	h (in)	L (in)	a/d	ρ_s	b_f (in)	t_f (in)	E_f (ksi)	S (ksi)	N_f	Failure Type
Heffernan 1997	3mLN1	6	12	112	4.7	0.018	-	-	-	54.5	730,000	FIRR
	3mLN2	6	12	112	4.7	0.018	-	-	-	39.9	1,063,000	FIRR
	3mMN1	6	12	112	4.7	0.018	-	-	-	39.4	290,000	FIRR
	3mMN2	6	12	112	4.7	0.018	-	-	-	57.3	350,000	FIRR
	3mHN1	6	12	112	4.7	0.018	-	-	-	65.7	160,000	FIRR
	3mHN2	6	12	112	4.7	0.018	-	-	-	47.1	130,000	FIRR
	5mNF	6	12	112	4.7	0.018	-	-	-	57.6	335,000	FIRR
	3mLC1	6	12	112	4.7	0.018	5	0.028	33794	39	4,890,000	FRP debonding following FIRR
	3mLC2	6	12	112	4.7	0.018	5	0.028	33794	30.6	6,440,000	FRP debonding following FIRR
	3mMC2	6	12	112	4.7	0.018	5	0.028	33794	56.8	890,000	FRP debonding following FIRR
	3mHSRC1	6	12	112	4.7	0.018	5	0.028	33794	52.3	340,000	FRP debonding following FIRR
	3mHSRC2	6	12	112	4.7	0.018	5	0.028	33794	48.2	390,000	FRP debonding following FIRR
	5mCF2	12	23	189	4.1	0.009	11.6	0.009	47137	51.2	312,000	FRP debonding following FIRR
	5mCF4	12	23	189	4.1	0.009	11.6	0.018	47137	50	627,000	FRP debonding following FIRR
	5mCF6	12	23	189	4.1	0.009	11.6	0.026	47137	37.1	n.r.	FRP debonding following FIRR
	3mMC1	6	12	112	4.7	0.018	5	0.028	33794	n.r.	900,000	FRP debonding following FIRR
Barnes and Mays 1999	1	5	9	90	5	0.013	-	-	-	40	20000	steel yield
	2	5	9	90	5	0.013	-	-	-	32	732,600	steel yield
	3	5	9	90	5	0.013	3.5	0.05	19597	39	508,500	FIRR
	4	5	9	90	5	0.013	3.5	0.05	19597	32	1,889,087	FIRR
	5	5	9	90	5	0.013	3.5	0.05	19597	26	11,968,200	run-out
Masoud et al. 2001	V	5	7	71	5.1	0.009	-	-	-	32.7	732,912	FIRR
	TIIF	5	7	71	5.1	0.009	4	0.039	n.r.	24.2	517,976	FIRR
Aidoo et al. 2004	U2	8.25	20	222	5.6	0.01	-	-	-	57.7	190,000	FIRR
	U3	8.25	20	222	5.6	0.01	-	-	-	29	2,000,000	FIRR
	U4	8.25	20	222	5.6	0.01	-	-	-	36.1	710,000	FIRR
	RS1	8.25	20	222	5.6	0.01	4	0.075	22500	49	308,879	FRP debonding following FIRR
	RF1	8.25	20	222	5.6	0.01	8	0.08	13900	44.4	193,160	FRP debonding following FIRR
	RS2	8.25	20	222	5.6	0.01	4	0.075	22500	40.4	1,280,000	FIRR

Table 1-1 (continued)

Researcher	Specimen	b (in)	h (in)	L (in)	a/d	ρ_s	b_f (in)	t_f (in)	E_f (ksi)	S (ksi)	N_f	Failure Type
Aidoo et al. 2004 (continued)	RF2	8.25	20	222	5.6	0.01	8	0.08	13900	40.4	960,000	FIRR
Quattlebaum	CS2 C-L(a)	6	10	180	9	0.01	2	0.055	22500	28.1	2,000,000	run-out specimen
et al. 2005	CS3 C-H	6	10	180	9	0.01	2	0.055	22500	31.7	523000	FIRR
Aidoo et al. 2006	unretrofit tee	13.5	32.5	336	5.2	0.028	-	-	-	16.5	2000000	run-out
	CAA tee	13.5	32.5	336	5.2	0.028	8	0.055	22500	14.3	2000000	run-out
Breña, Wood and	AF2	8	14	106	3.8	0.006	2	0.013	33000	19.7	1000000	run-out
Kreger 2002	AF3	8	14	106	3.8	0.006	2	0.013	33000	34.8	1000000	run-out
	AF4	8	14	106	3.8	0.006	2	0.013	33000	60.9	155950	FRP debonding following FIRR
	BF1	8	16	118	3.7	0.005	2	0.047	22500	29	1000000	run-out
	BF2	8	16	118	3.7	0.005	2	0.047	22500	43.5	1000000	run-out
	BF3	8	16	118	3.7	0.005	2	0.047	22500	62.9	55490	fatigue-induced FRP debonding
	BF4	8	16	118	3.7	0.005	2	0.047	22500	62.9	8990	fatigue-induced FRP debonding
Papakonstantinou	N4	6	6	48	4	0.015	-	-	-	25.8	2,000,000	run-out
et al. 2001	N5	6	6	48	4	0.015	-	-	-	30.2	2,000,000	run-out
	N8	6	6	48	4	0.015	-	-	-	39.7	650,000	FIRR
	N3	6	6	48	4	0.015	-	-	-	46.9	275,000	FIRR
	N6	6	6	48	4	0.015	-	-	-	54.1	155,000	FIRR
	N7	6	6	48	4	0.015	-	-	-	65.3	80,000	FIRR
	S11	6	6	48	4	0.015	6	0.014	10500	33.9	6,000,000	run-out
	S10	6	6	48	4	0.015	6	0.014	10500	38.1	685,000	FRP debonding following FIRR [1]
	S2	6	6	48	4	0.015	6	0.014	10500	39	880,020	FRP debonding following FIRR [1]
	S5	6	6	48	4	0.015	6	0.014	10500	39.9	800,000	FRP debonding following FIRR [1]
	S7	6	6	48	4	0.015	6	0.014	10500	42.9	570,000	FRP debonding following FIRR [1]
	S9	6	6	48	4	0.015	6	0.014	10500	49.7	235,000	FRP debonding following FIRR [1]
	S6	6	6	48	4	0.015	6	0.014	10500	55.7	126,000	FRP debonding following FIRR [1]
	S8	6	6	48	4	0.015	6	0.014	10500	64.2	30,500	FRP debonding following FIRR [1]
Gussenhoffen	A1480	4	4	34	3.5	0.013	3.5	0.007	37710	42.8	131,619	concrete cover peel off
and Breña 2005	A1470	4	4	34	3.5	0.013	3.5	0.007	37710	39.4	287,594	FRP debonding following FIRR
	A1460	4	4	34	3.5	0.013	3.5	0.007	37710	32.5	778,734	FIRR and concrete cover peel off

Table 1-1 (continued)

Researcher	Specimen	b (in)	h (in)	L (in)	a/d	ρ_s	b_f (in)	t_f (in)	E_f (ksi)	S (ksi)	N_f	Failure Type
Gussenhoffen and Breña 2005 (continued)	B1280	4	4	34	3.5	0.013	2	0.007	37710	43.5	290,307	FRP debonding following FIRR
	B1270	4	4	34	3.5	0.013	2	0.007	37710	38.9	336,873	FRP debonding following FIRR
	B1260	4	4	34	3.5	0.013	2	0.007	37710	34.2	4,000,000	run-out
	B2270	4	4	34	3.5	0.013	2	0.013	37710	39.2	150,000	concrete cover peel off
	B2260	4	4	34	3.5	0.013	2	0.013	37710	28.9	2,000,000	run-out
	C1280	4	4	34	3.5	0.013	2	0.007	37710	47.3	326,775	FRP debonding following FIRR
	C1270	4	4	34	3.5	0.013	2	0.007	37710	32.8	440,193	FRP debonding following FIRR
	C1260	4	4	34	3.5	0.013	2	0.007	37710	27.4	4,000,000	run-out
	A-control	4	4	34	3.5	0.013	-	-	-	45	183674	FIRR
Zorn 2006	CF	6	10	186	9.3	0.01	-	-	-	34.8	>329324	test lost at cycle 329324
	L1F	6	10	186	9.3	0.01	1	0.055	22500	35.9	400867	FIRR
	L2F	6	10	186	9.3	0.01	2	0.055	22500	30	2000000	run-out
	L2x1F	6	10	186	9.3	0.01	2	0.055	22500	30	447695	FIRR
	L4F	6	10	186	9.3	0.01	4	0.055	22500	25.2	2000000	run-out
	H1F	6	10	186	9.3	0.01	1	0.055	22500	34.7	424422	FIRR
	H2F	6	10	186	9.3	0.01	2	0.055	22500	28.9	1128006	FIRR
	H2x1F	6	10	186	9.3	0.01	2	0.055	22500	31.9	2000000	run-out
	H4F	6	10	186	9.3	0.01	4	0.055	22500	25.4	2000000	run-out

[1] FRP extended over beam and was thus "anchored" by reaction force.
FIRR = fatigue-induced reinforcing steel rupture.
n.r. = not reported
run-out = fatigue test stopped at reported N; run-out tests are typically followed by a monotonic test to failure.

Table 1-2 Summary of current guidelines for maximum allowable stress in bonded FRP subject to fatigue loading.

	Carbon FRP	Glass FRP	Aramid FRP
ACI 440.2R-02	$f_{fuf} < 0.55f_{fu}$	$f_{fuf} < 0.20f_{fu}$	$f_{fuf} < 0.30f_{fu}$
Concrete Society TR55	$f_{fuf} < 0.80f_{fu}$	$f_{fuf} < 0.30f_{fu}$	$f_{fuf} < 0.70f_{fu}$
JSCE recommendations	$f_{fuf} < \mathbf{0.84}f_{fud}$		
CNR 200/2004	$f_{fuf} < \mathbf{0.50}f_{fud}$		
CEB Bulletin 14	none		
f_{fuf} stress limit in FRP under fatigue load conditions f_{fu} ultimate capacity of FRP f_{fud} allowable stress in FRP to mitigate debonding			

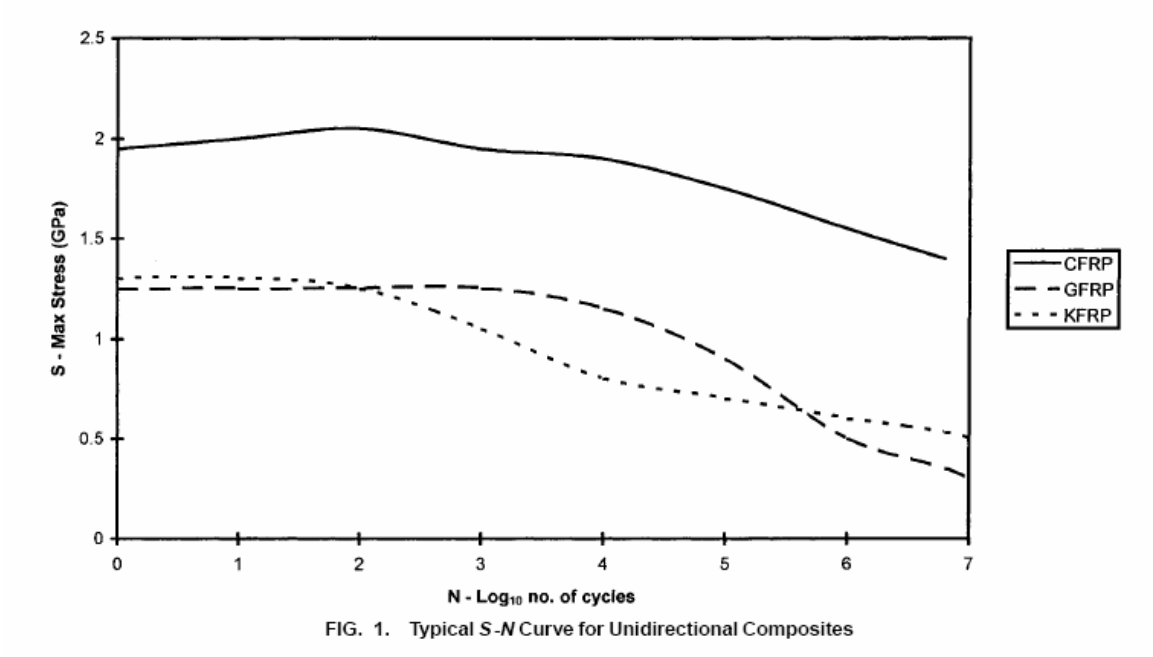

Figure 1-1 Representative S-N relationships for FRP materials
(Barnes and Mays, 1999)

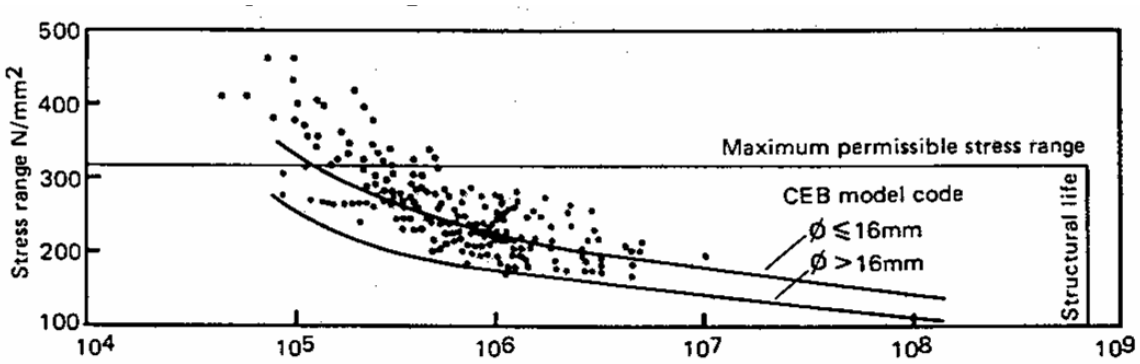

Figure 1-2 Representative S-N relationships for steel reinforcing bars
(Tilly and Moss, 1982)

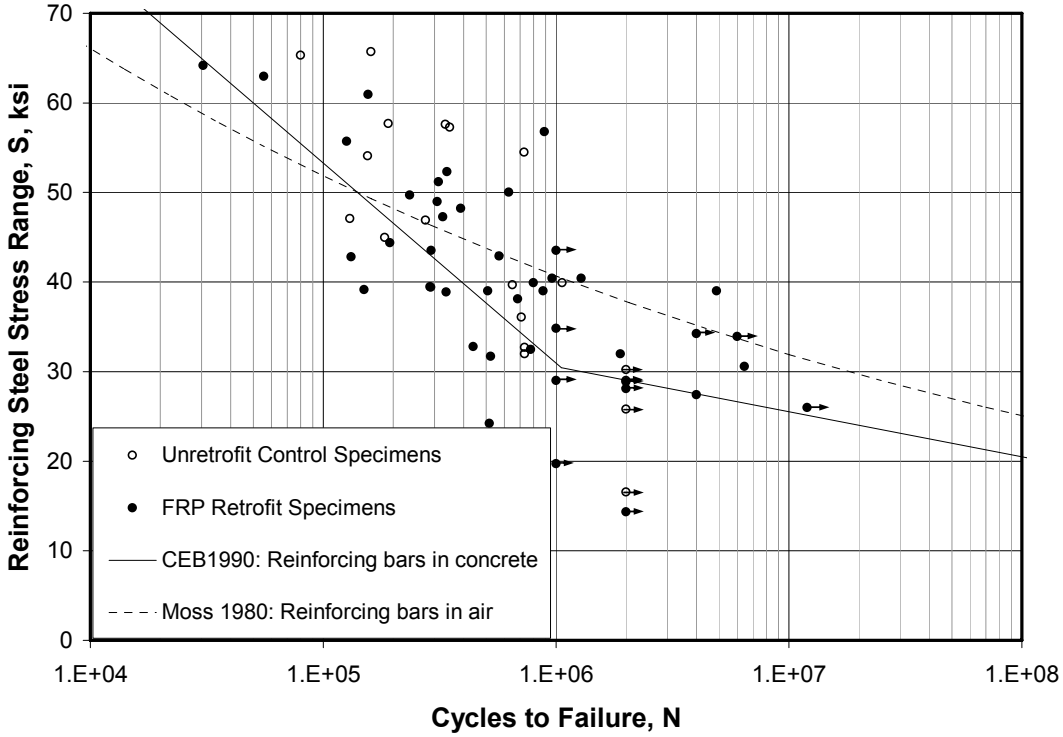

Figure 1-3 S-N data for test reported in available literature

2.0 EXPERIMENTAL PROGRAM

This chapter reports details of the experimental program. The CFRP application, test setup, and instrumentation are also presented in Reeve (2005) and repeated here for completeness and clarity.

2.1 REINFORCED CONCRETE BEAM TEST SPECIMENS

There were twenty-four reinforced concrete beams cast. Of these, eight were retrofitted with carbon fiber reinforced polymer (CFRP) composite strips and tested monotonically to failure (Reeve, 2005). The results from the monotonic testing were used to design the experiments conducted in this research. Another eight of these beams were retrofitted identically to the monotonic specimens and tested under fatigue loading to failure or 2 million cycles. Those beams that remained intact after 2 million cycles were then tested monotonically to failure. Additionally, two unretrofit control specimens were tested, one monotonically (Reeve 2005) and one in fatigue. The remaining four beams were tested with a different retrofit scheme and are presented in a different study (Minnaugh, 2006). All beams were 10" (254 mm) deep by 6" (152 mm) wide and were cast with concrete having a measured 28-day compressive strength, f_c', equal to 3384 psi (23.3 MPa) and a maximum coarse aggregate size of 1.5" (37 mm). Three #4 reinforcing bars were used as primary tension reinforcement and two #3 bars were used in the compression zone of the beam. The compression bars were provided so that beams could be inverted for the application of the CFRP. The beams were cured in their forms for seven days before being removed and stored in the ambient laboratory environment. The beams cured in these ambient conditions for more than 56 days before they were moved and inverted for the

CFRP application. Material properties for the reinforcing steel and concrete are presented in Table 2-1. Figure 2-1 shows a detailed drawing of the beam design.

2.2 RETROFIT MEASURES

There were eight different retrofit measures conducted in this study. Four CFRP strip arrangements were used in combination with two adhesive types. The adhesives used were Sikadur 23 and Sikadur 30. Material properties for these adhesives are presented in Table 2-2. Sikadur 23 is referred to as the low-modulus epoxy (denoted L) in this study and Sikadur 30 is the high-modulus epoxy (denoted H). Sikadur 30 is approximately twice as stiff as Sikadur 23, as indicated in Table 2-2. Only Conventional Adhesive Applied (CAA) FRP systems are used in this study. The retrofit material used was Fyfe UC strips. Material properties for the CFRP strips can be found in Table 2-3. Fyfe UC strips come as a continuous 4" (102 mm) wide, 0.055" (1.4 mm) thick roll. The strips are easily split longitudinally using a straight razor and cut transversely using aviation shears. Four strip arrangements were used as shown in Figure 2-2: 4" (102 mm), 2" (51 mm), and 1" (25 mm) and 2 x 1" strips were used. The single strips were applied along the longitudinal center line of the beam while the two 1" strips were centered on the beam with a 2" (51 mm) gap between them. One beam was prepared in each case using the high-modulus epoxy and the other using the low-modulus epoxy. The retrofit schemes are shown in Figure 2-2. Details of the CFRP application are located in the following sections.

2.3 CAA APPLICATION OF CFRP TO THE TEST SPECIMENS

After the 56 day compressive strength tests, the retrofitting process was begun. This allowed for adequate concrete curing time before handling and inverting of the RC beams. Additionally, this curing time in ambient conditions will have effectively dried out the surface region of the concrete. The application of the CFRP strips to the tension faces of the beams is

explained in this section. There were sixteen beams retrofitted with CFRP having four configurations as discussed in Section 2.2.

2.3.1 Concrete Surface Preparation

Before any CFRP could be applied to the concrete surface of the beams, the surface had to be prepared in accordance with the recommendations of the adhesive and CFRP manufacturers. The surface was prepared using an angle grinder with a wire wheel attachment to remove all laitance and dirt from the working surface of the concrete beam. Compressed air was then used to remove any concrete dust and dirt that settled on the beam. The final beam surface resembled ICRI Concrete Surface Profile 3.

2.3.2 Preparation of the CFRP Material

The CFRP was cut into 172" (4369 mm) lengths with aviation shears and cut longitudinally with a straight razor as needed. Once the CFRP was cut, it was stored and protected from dust, dirt and mechanical damage.

2.3.3 Application of the CFRP Reinforcement

Once the CFRP was cut to width and length and the concrete surface prepared, the CFRP was ready for application. With the beams inverted and having an unobstructed working surface on the tension face of the beam, the retrofit process was begun. Sixteen beams were retrofitted. Eight were using the Sikadur-30 epoxy and the other eight using the Sikadur-23 epoxy. Each resin was mixed according to the manufacturers specifications and applied within the pot life of each epoxy system. Using plastic spatulas, the epoxy was applied over the length of the beam, ensuring that all the surface area in contact with CFRP had a layer of epoxy. The CFRP strips were laid out and epoxy was applied to the matte or textured (resin-poor) side of the strip. Once the strips and the beams had the epoxy resin applied to them, the strips were then laid down on

the longitudinal centerline of the beam. Starting on the centerline of the beam and moving outward toward the supports locations, the strips were pressed onto the concrete with uniform pressure from rollers and fingertips.

2.4 SPECIMEN DESIGNATION

Of the eighteen beams considered within the scope of the thesis, all had different designations. The designation system is as follows:

XYZ

Where X stands for the epoxy system:

C = unretrofit control beam

H = high-modulus epoxy (Sikadur 30)

L = low-modulus epoxy (Sikadur 23)

Where Y stands for the CFRP strip width and configuration:

1 = 1” (25 mm) wide strip

2 = 2” (51 mm) wide strip

2x1 = two 1” (25 mm) wide strips

4 = 4” (102 mm) wide strip

And Z indicates the loading type:

blank = monotonic loading (tested by Reeve, 2005)

F = fatigue loading as described in Section 2.7

An example would be the H1F specimen. This is the beam with a 1" (25 mm) CFRP adhered to the tension face of the beam with the high modulus resin and tested under fatigue loading.

2.5 TEST SETUP

All beams were tested under cyclic mid-point bending. An MTS hydraulic actuator with a capacity of 50 kips (222 kN) and a stroke of 4" (102 mm) was used. The 186.5" (4737 mm) long beams were supported over a clear span of 178.25" (4527 mm). The supports consisted of a 3" x 6" x ½" (76 mm x 152 mm x 13 mm) neoprene pad on a 3/8" (9 mm) steel plate on a steel roller. The neoprene pads had a durometer rating of 65-75. The steel plates on steel rollers created true simply supported conditions. At the loading point at mid-span of the beam, the same size neoprene pad was used to minimize local crushing of the concrete. Under cyclic loading, significant damage would result from a steel to concrete interface at both the supports and the loading point. A photograph of the test setup is shown in Figure 2-3.

2.6 INSTRUMENTATION

All beams had the same instrumentation shown in Figure 2-4. Each beam was instrumented with four electrical resistance strain gages located on the middle #4 reinforcing bar. These gages had a spacing of 12" (305 mm) center-to-center and were centered on mid-span. The mid-span displacement of each beam was measured with a draw wire transducer.

The retrofitted specimens were instrumented with an additional four strain gages mounted on the external surface of the CFRP strips. They were located on 12" (305 mm) spacing corresponding to the location of the gages on the internal reinforcing steel. Additional gages were provided on the 4" (102 mm) wide CFRP strips (Reeve, 2005) although data from these is not reported in this thesis.

The MTS hydraulic actuator was equipped with an internal linear variable displacement transducer (LVDT) and a 50 kip (222 kN) load cell. All strain gages, the load cell, draw-wire transducer, and LVDT were connected into a Vishay System 5100 data acquisition system. The

controller used for these tests was an MTS FlexTest SE hydraulic servo-controller. A schematic of the instrumentation can be found in Figure 2-4.

2.7 TEST PROCEDURE

Nine reinforced concrete beams were tested under cyclic mid-point bending over a span of 178.25" (4527 mm). One specimen was not retrofitted with CFRP and was used as a control beam. The remaining eight beams were retrofitted and tested to failure or two million cycles under fatigue loading at a frequency not exceeding 1.7 Hz. All cyclic tests were run in load control. The applied mid-span load was cycled from 1 kip (4.45 kN) to 5 kips (22.24 kN) in a sinusoidal wave form. Testing proceeded twenty-four hours per day, seven days a week. This was done so the tests could be completed in a timely manner and also to mitigate the possibility of damage recovery between cycling periods. When data was being recorded, the test was slowed to 1.2 Hz, the highest frequency at which quality data could be taken. When data was not being recorded, the frequency was increased to 1.7 Hz. This rate permitted excellent sustained control over both the lower (1 kip) and upper (5 kip) peak loads. The data acquisition sampling rate was 50 samples per second. The interval at which data was recorded was kept under 100,000 cycles. Usually, a set of data was taken in the morning and in the late evening. Table 2-4 provides the intervals at which data was recorded for each specimen. Due to equipment failure during testing, the unretrofit control beam was destroyed after only 329,324 cycles of fatigue loading and thus this specimen is not reported here.

2.7.1 Selection of Fatigue Load Levels

The fatigue loading scheme used – cycling from 1 to 5 kips - was selected based on the measured reinforcing bar strains from the original monotonic control Specimen C reported by Reeve (2005). The 1 kip lower limit was selected to represent a continuously applied dead load

and the 5 kip upper limit was selected to achieve the desired strain range (and hence stress range) in the reinforcing steel. The target strain range in the steel reinforcement was 1200 με and the resulting stress range was 34.8 ksi (240 MPa). Using some representative S-N relationships, the target stress range was verified to result in fatigue critical loading conditions but not low-cycle fatigue. The target fatigue life of the unretrofit control beam was selected to fall between N = 100,000 and N = 1,000,000. The equations used to estimate the fatigue stress range are presented below:

For uncorroded steel reinforcement embedded in concrete, Mallet (1991) recommends:

$$S^9 N = 1.539 \times 10^{27} \quad \text{(S in MPa units)} \qquad (2\text{-}1)$$

Tilly and Moss (1982) report an empirically derived relationship for reinforcing bars 0.63 in. (16 mm) in diameter or smaller embedded in concrete beams tested in flexure:

$$S^9 N = 3.09 \times 10^{27} \quad \text{(S in MPa units)} \qquad (2\text{-}2)$$

For reinforcing bars smaller than 0.63 in. (16 mm) in diameter embedded in concrete and tested at stress ranges expected to result in a fatigue life N < 1,000,000, CEB/FIB (1990) recommend:

$$S^5 N = 4.0841 \times 10^{17} \quad \text{(S in MPa units)} \qquad (2\text{-}3)$$

A lower bound S-N behavior is estimated using a relationship established for testing reinforcing steel in direct tension in air. The equation proposed by Helgason and Hanson (1974) is used in this case:

$$\log(N) = 6.969 - 0.383S \quad \text{(S in ksi units)} \qquad (2\text{-}4)$$

Previous studies (Quattlebaum et al., 2005) have shown Equation 2-3 to be most representative and Equation 2-2 to represent an upper bound S-N behavior for the limited data available as presented in Chapter 1. Equations 2-2 and 2-3 are represented in Figure 1-3. The

predicted and actual fatigue life of all nine specimens considered in this study is shown in Table 2-5.

2.7.2 Fatigue Run-out Specimens

Four of the beams remained intact following two million cycles of fatigue loading. At this point, the test was stopped and a monotonic cycle to failure was conducted. The procedure for the monotonic cycle is identical to the procedure outlined in the companion thesis (Reeve, 2005). The push to failure was done in stroke control and programmed to push the beam from zero mid-span displacement to the full actuator displacement (4" (102 mm)) in two hours. The data acquisition was programmed to sample at a rate of 1 sample every 2 seconds during this loading. In these cases, the specimens may be considered "fatigue conditioned" monotonic tests comparable to those reported by Reeve (2005).

2.7.3 Specimen L4F

Similar to Reeve's L4 specimen, the L4F specimen was used as a vehicle for the testing of an innovative instrumentation scheme aimed at monitoring the quality of the bond between the CFRP and the concrete (Kim et al., 2006). In addition to slowing the test down while recording data, the test had to be stopped for approximately ten minutes a day. The specialized instrumentation required that a constant load be applied to the beam and that the beam be stationary while recording data. The minimum load of 1 kip (4.448 kN) was applied to the beam at all times while the test was stopped.

Specimen L4F turned out to be a run-out specimen, so different test procedures also had to be followed for the final monotonic cycle. This procedure was identical to that used for the original L4 monotonic test (Reeve, 2005). When two million cycles were reached, the controller was put in load control and the load was reduced to 1 kip (4.448 kN). This load level was held

for approximately 10 minutes while data was being recorded. The load was then sequentially increased to 3 kips (13.34 kN), 5 kips (22.24 kN), 7 kips (31.36 kN), and 9 kips (40.03 kN). At all of these stopping points the load was held so that data could be acquired. Following 9 kips (40.03 kN), the controller was put in stroke control and set to move the actuator to full stroke in two hours. This allowed data to be recorded during the testing. This slower test procedure is not believed to have affected the results in any significant manner. It is possible that the resulting test displacements may be increased marginally under this slower test, although this cannot be verified (Reeve, 2005).

Table 2-1 Experimentally determined concrete and reinforcing steel material properties

Specimen	28 Day Concrete Strength	Age at Time of Beam Test	Reinforcing Steel
	psi (MPa)	days	ksi (MPa)
CF	f_c' = 3384 (23.3)	175	E = 30000 ksi (206842)
L1F		184	
L2F		191	
L2x1F		231	f_y = 62.2 (429)
L4F		274	
H1F		210	
H2F		217	f_u = 96.8 (667)
H2x1F		238	
H4F		253	

Table 2-2 Manufacturer's reported properties of adhesive systems used (SIKA, 2005).

Property	ASTM test method	Sikadur 23	Sikadur 30
tensile strength, ksi (MPa)	D638	2.0 (14)	3.6 (25)
tensile modulus, ksi (MPa)		323 (2227)	650 (4482)
elongation at rupture		0.063	0.010
modulus of rupture, ksi (MPa)	D790	4.8 (33)	6.8 (47)
tangent modulus of elasticity, ksi (MPa)		471 (3247)	1700 (11721)
shear strength, ksi (MPa)	D732	3.0 (21)	3.6 (25)
bond strength, ksi (MPa)	C882	2.6 (18)	3.2 (22)
compressive strength, ksi (MPa)	D695	5.2 (36)	8.6 (59)
compressive modulus, ksi (MPa)		128 (883)	390 (2689)

Table 2-3 Manufacturer's reported properties of CFRP strips (Fyfe, 2005).

Property	ASTM test method	UC Strip
tensile strength, ksi (MPa)	D3039	405 (2792)
tensile modulus, ksi (MPa)		22500 (155138)
elongation at rupture		0.018
perpendicular strength, psi (MPa)		negligible
strip thickness, in. (mm)	na	0.055 (1.4)
widths used in testing, in. (mm)	na	1 (25); 2 (51); 4 (102)

Table 2-4 Cycle numbers at which data was recorded for each specimen

CF	L1F	L2F	L2x1F	L4F	H1F	H2F	H2x1F	H4F
1	1	1	1	1	1	1	1	1
4	4	28	42	48	87	60	33	57
41	14	30	68	201	201	208	201	117
53	204	100	200	516	501	500	506	205
80	504	203	514	1001	1002	1000	1003	501
203	1002	503	1000	2000	2003	2002	2002	1001
503	1052	1000	2000	5122	5003	5002	5000	2005
1003	2001	2002	5002	10013	10001	10000	12345	5014
2004	2024	5000	20006	26302	24125	17536	22263	10014
5004	5001	9005	49921	78613	45328	48309	41728	36036
10003	5042	26175	93754	134314	85181	76518	74672	46734
23000	10002	53644	129884	185860	107847	105945	105084	79271
25003	10097	97371	186508	221836	140871	127367	134019	118213
50001	14566	139081	243456	280885	185247	174010	180804	163295
80630	15002	171802	286524	318556	199452	193373	221546	225503
100003	15025	198997	333084	374834	224443	244356	263148	278005
118835	22814	252293	387071	430022	257143	288365	330456	315878
150008	25005	306074	447695	448835	257450	309744	383080	376699
163210	25022	339047	472642	502791	291880	332931	408711	417599
175016	50002	394505	478203	563620	292080	363267	457917	449137
200003	50027	448168		608632	333534	384397	491206	507291
232341	82533	516204		649613	395888	456885	543094	552741
250005	82595	548306		720331	396375	499343	587368	603916
260560	82740	614758		786076	408978	530053	634543	671912
263864	100002	649379		853999	424422	584658	680704	755767
288703	100034	678344		889353	442466	634809	727082	807005
288795	108595	718318		931229	442982	683506	770932	846760
288869	108621	796748		1002712	452766	725006	795840	890684
319910	120308	850088		1030549	479068	769108	857770	953164
319940	120328	932773		1090374	479274	829105	888616	975352
319972	138727	999057		1148406	506593	870311	921602	1040486
320754	138753	1104642		1183660	538653	900472	956056	1100111
	172711	1104779		1233362	576617	929177	1010641	1149453
	172732	1153058		1299987		981210	1046631	1187032
	188970	1208866		1342193		1026397	1091782	1237245
	188993	1233708		1421784		1064437	1150133	1286794
	225002	1270711		1443799		1128006	1195622	1340744
	225028	1313465		1481058		1191770	1249275	1398812
	252821	1331586		1562563		1213229	1308834	1416507
	252844	1370787		1593515		1244102	1339340	1479046
	287103	1428332		1649520			1395821	1532647
	287125	1480351		1698459			1440043	1578044
	311397	1497354		1763351			1469580	1623563
	311421	1513597		1799316			1522985	1704778
	342629	1551888		1870298			1582672	1767744
	342652	1589683		1895925			1626337	1824631
	370507	1613127		1997194			1682752	1869105
	370532	1644243		2000000			1737853	1924854
	400867	1698454					1774778	1978593
	400892	1778638					1820072	2000000
	432933	1838827					1882516	
	432970	1882825					1928895	
		1924840					1965616	
		2000000					1966273	
							1998684	
							2000000	

Table 2-5 Predicted and Actual Fatigue Life of all specimens

	initial ε range (με)	**initial S** (ksi)	**Observed N**	**Equation**			
				2.1.	**2.2.**	**2.3.**	**2.4.**
Target	1200	35	NA	583737	1172025	513486	432673
CF	1203	35	>329324[1]	570324	1145094	506898	429253
L1F	1237	36	400867	444141	891745	441150	393608
L2F	1035	30	2000000	2209963	4437158	1075804	659820
L2x1F	1036	30	447695	2190839	4398760	1070622	658135
L4F	870	25	2000000	10548117	21178480	2563532	1006215
H1F	1195	35	424422	606090	1216906	524319	438241
H2F	996	29	1128006	3122584	6269516	1303582	729026
H2x1F	1101	32	2000000	1266958	2543795	789766	557339
H4F	877	25	2000000	9814131	19704786	2462845	988362

[1]Specimen loaded to failure due to equipment malfunction

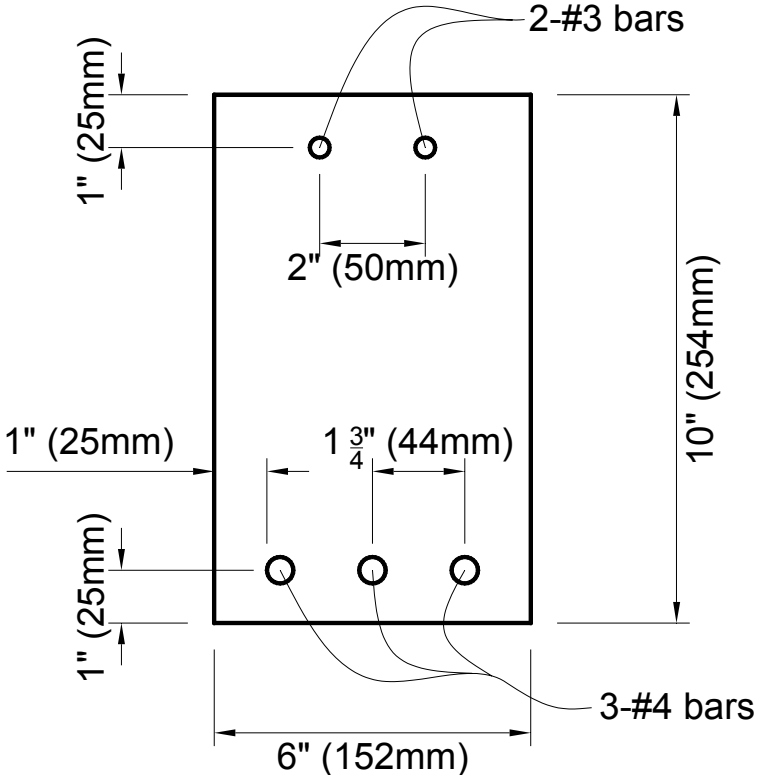

Figure 2-1 Detail of reinforced concrete beam specimens.

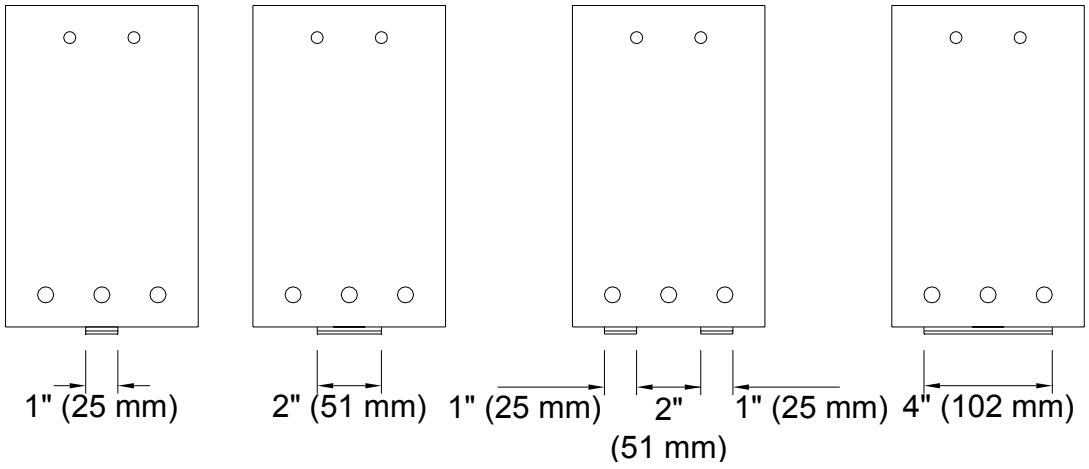

Figure 2-2 Detail of centered CFRP strips (a uniform adhesive layer approximately 1/16" (1.6 mm) thick was used in each case to adhere the CFRP).

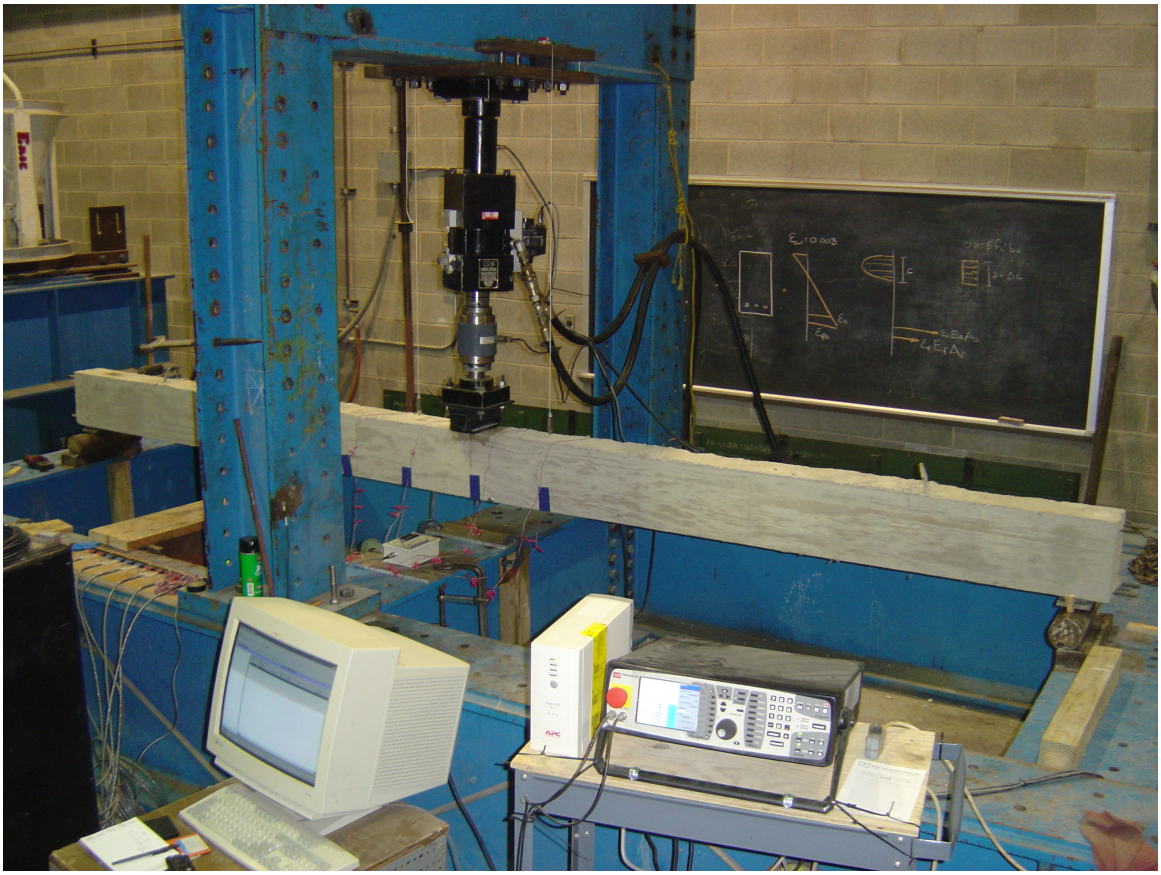

Figure 2-3 Photograph of test setup

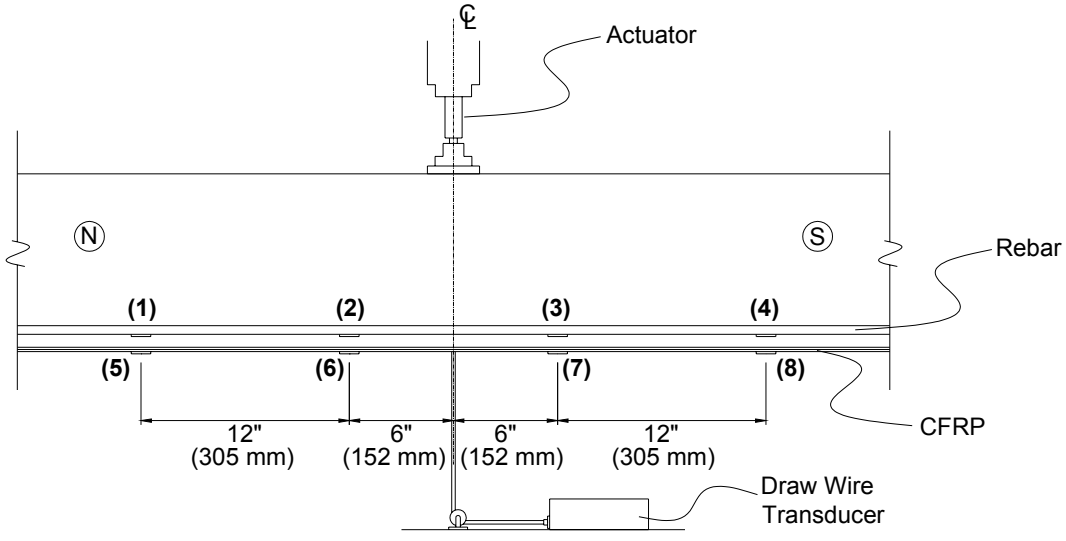

Figure 2-4 Schematic of instrumentation.

3.0 TEST RESULTS AND TYPICAL SPECIMEN BEHAVIOR

This chapter presents the results of the test program and explains the behavior of each test specimen.

3.1 TEST RESULTS

Figures 3-1 thru 3-8 show load vs. midspan deflection graphs for each retrofitted test specimen in comparison with the control specimen, Specimen C, and the companion retrofitted monotonic specimen (both control specimens are reported by Reeve, 2005). In each figure, representative instrumented fatigue cycles are shown in addition to the final monotonic load to failure for those specimens (L2F, L4F, H2x1F and H4F) reaching 2 million fatigue cycles. Figure 3-9 shows the damage accumulation, as measured by midspan deflection, with cycling for all eight retrofit specimens. The midspan displacements for each specimen are shifted vertically 0.5 inches from each other for clarity. Strain vs. cycle number damage accumulation curves are shown for each test specimen in Figures 3-10 thru 3-17b. Coincident reinforcing bar and CFRP strains are shown plotted on the same axes. The strains at each location axially along the specimens are shifted vertically 2000 microstrain for clarity. Figures 3-18 thru 3-21 show load vs. reinforcing bar and CFRP strain for the run-out monotonic tests. Figure 3-22 is a photograph of a typical fatigue-induced rupture of a #4 reinforcing bar seen during this test program. The cleaved failure with no apparent necking or “cup and cone” failure surfaces is indicative of fatigue failure. Figure 3-23 is a typical example of crack induced debonding. Figure 3-24 is the SN curve of all available data including the data of this test program.

A summary of the key results for the fatigue testing of all test specimens is presented in Table 3-1. Table 3-2 presents the key results for the final monotonic cycle for the fatigue run-out specimens, L2F, L4F, H2x1F, and H4F.

The following are definitions for the data reported in Table 3-1:

b_f/b: ratio of gross CFRP width to concrete substrate width (widths shown in Figure 2-2)

age: age, in days, at time of testing since test specimen was cast. CFRP was applied at an age of approximately 56 days in all cases.

cracking load: midspan loading at initiation of initial concrete cracking, as determined from first abrupt increase in reinforcing bar strain for each test specimen.

The following parameters are reported for the first instrumented fatigue cycle, N = 2, and the final instrumented fatigue cycle, N_f. For those specimens experiencing run-out at 2 million cycles, N_f = 2 million.

minimum applied load: minimum midspan loading carried by a test specimen during one fatigue cycle (target = 1 kip).

deflection at minimum applied load: corresponding midspan deflection at the minimum applied load during instrumented cycles N = 2 and N = N_f.

maximum reinforcing bar strain at minimum applied load: corresponding maximum reinforcing bar strain (instrumented middle rebar) at the minimum applied load during instrumented cycles N = 2 and N = N_f.

maximum FRP strain at minimum applied load: corresponding maximum CFRP strain at the minimum applied load during instrumented cycles N = 2 and N = N_f.

maximum applied load: maximum midspan loading carried by a test specimen during one fatigue cycle (target = 5 kips).

deflection at maximum applied load: corresponding midspan deflection at the maximum applied load during instrumented cycles N = 2 and N = N_f.

maximum reinforcing bar strain at maximum applied load: corresponding maximum reinforcing bar strain (instrumented middle rebar) at the maximum applied load during instrumented cycles N = 2 and N = N_f.

maximum CFRP strain at maximum applied load: corresponding maximum FRP strain at the maximum applied load during instrumented cycles N = 2 and N = N_f.

range of applied load: the difference between the minimum applied load and the maximum applied load.

stress range in reinforcing bar: using E = 29000 ksi (200 GPa), the stress range is calculated from the minimum and maximum reinforcing bar strains.

stress range in FRP: using E = 22500 ksi (155 GPa), the stress range is calculated from the minimum and maximum CFRP strains.

apparent stiffness: calculated as the secant stiffness between the minimum and maximum applied loads for instrumented cycles N = 2 and N = N_f.

The following parameters reflect values that occur at any time during the fatigue cycling; i.e.: N < N_f:

maximum observed strain in FRP: the greatest strain observed in the CFRP during the course of fatigue cycling. The strain in the corresponding reinforcing bar recorded at the same time is also indicated.

initiation of CFRP debonding: The CFRP strain at which debonding apparently initiates as determined by comparing strain time histories of the CFRP strips and corresponding reinforcing bars. Additional knowledge of the debonding mechanism is also assumed as described in Reeve

(2005). It is hypothesized that debonding will initiate near midspan in the region between CFRP gauges (5) and (6) or (7) and (8). Debonding, once initiated, will propagate away from the midspan toward the support. Thus, as the debonding propagates past the point of the outermost CFRP gauges, (5) or (8), the strains in these gauges should increase relative to their corresponding reinforcing bars, (1) and (4). This increase is due to the loss of shear transfer along the debonded region. The incremental stress usually transferred by the bond is now uniformly transferred across the debonded CFRP and is anchored beyond the debonded region. Observations of beam behavior and eventual complete debonding are used to verify the location of debonding identified by the strain data. An illustrative example of this method can be found in Reeve (2005).

The following additional parameters are reported in Table 3-2:

load at initial yield: midspan loading corresponding to the middle #4 tensile reinforcing bar attaining a strain of 2140 microstrain (yield strain value for reinforcing steel based on experimentally obtained yield stress data (see Table 2-1) and calculated assuming E = 29,000 ksi (200 GPa)).

load at general yield: midspan loading at which general yield of the specimen occurred, defined as a significant change in stiffness of the load vs. deflection curve with observable nonlinearity. Since the stiffness of the load vs. deflection response decays gradually, general yield is determined as the intersection of the cracked elastic tangent stiffness and the post-yield stiffness resulting in the same area under the load-deflection curve. An illustrative example of this determination can be found in Reeve (2005).

strain in CFRP at general yield: maximum strain in CFRP at time of general yield deflection.

maximum load: maximum midspan loading carried by a test specimen during monotonic testing.

ultimate load: the greater of: the load corresponding to failure of the specimen, or the load at which the load carrying capacity falls below 80% of the maximum load obtained.

ductility: ratio of the deflection at the ultimate load to the deflection at general yield.

maximum CFRP strain: the greatest strain in the CFRP observed. The strain in the corresponding reinforcing bar recorded at the same time is also indicated.

initiation of debonding: The FRP strain at which debonding apparently initiates as described above.

All moments given in Tables 3-1 and 3-2 are the midspan moments, determined from their corresponding midspan loading. The moments are determined from statics as PL/4 where L is the clear span of the beam, 178⅝" (4537 mm), and P is the midspan load. All deflections given in Tables 3-1 and 3-2 are the midspan deflections measured at the corresponding midspan loading.

3.2 SPECIMEN BEHAVIOR

This section discusses the behavior of each test specimen.

3.2.1 Specimen L1F

The testing of Specimen L1F resulted in a fatigue-induced reinforcing bar rupture. The stiffness of Specimen L1F and companion Specimen L1 were nearly identical. This can be seen in Figure 3-1. The rupture of the east reinforcing bar became apparent after cycle 400,867. At this point, the stiffness of the beam changed significantly and an increase in midspan deflection was evident. There was also significant cracking near midspan due to the energy release associated with a fatigue rupture and the greater beam deformations. The test was continued until

cycle 433,378, at which the west reinforcing bar ruptured and the CFRP debonded. The failure mode of Specimen L1F was fatigue-induced reinforcing steel rupture; debonding of the CFRP following steel rupture is a secondary failure associated with the immediate transfer of stress from the reinforcing steel to the CFRP.

3.2.2 Specimen L2F

Specimen L2F sustained 2,000,000 cycles of fatigue loading, at which point fatigue testing was terminated and a final monotonic test was run to fail the beam. Specimen L2F was slightly stiffer than the companion Specimen L2. This can be seen in Figure 3-2. The specimen was cycled to 2,000,000 cycles with very little apparent damage accumulation and no apparent debonding. A "tap test" (literally, tapping the CFRP with a small object and listening for the different pitch indicating sound bond or debonded CFRP) was done on the CFRP strips to determine where, if any, debonding may have occurred. The tap test revealed no debonding. The monotonic test resulted in nearly identical load-deflection and failure behavior to the monotonic Specimen L2. Specimen L2F exhibited a large shear failure/splitting failure. Debonding initiated at the toe of the shear crack and progressed towards the south support. A photograph of this debonding behavior can be seen in Figure 3-23 (the splitting failure shown in Figure 3-23 is a secondary post-failure effect). Complete debonding of the CFRP strip did not occur, as it remained bonded near the south support. Specimen L2F had an ultimate capacity of 10.23 kips (45.5 kN). The load vs. strain plot for Specimen L2F can be found in Figure 3-18.

3.2.3 Specimen L2x1F

The testing of Specimen L2x1F resulted in a fatigue-induced reinforcing bar rupture. The stiffness of Specimen L2x1F and companion Specimen L2 were nearly identical. This can be seen in Figure 3-3. The rupture of the west reinforcing bar became apparent after cycle 447,695.

At this point, the stiffness of the beam changed significantly and an increase in midspan deflection was evident. The rupture was also evident from the behavior of the existing crack in the vicinity of the rupture location. The width of the crack increased significantly following rupture of the reinforcing steel. The fatigue test was terminated following the reinforcing steel rupture. A tap test was performed to determine the extent of debonding. Debonding was only identified from midspan of the beam extending 4 in. (100 mm) south of midspan. The reinforcing bar rupture was located 2.25 in. (57 mm) south of midspan. This local debonding may be attributed to damage caused by the energy release from the reinforcing bar rupture. Because the debonding did not apparently extend past the strain gage locations at 6 and 18 inches (152 and 457 mm) from midspan, instrumentation evidence of debonding will not be attainable for this test. The failure mode of Specimen L2x1F was fatigue-induced reinforcing steel rupture.

3.2.4 Specimen L4F

Specimen L4F sustained 2,000,000 cycles of fatigue loading, at which point fatigue testing was terminated and a final monotonic test was run to fail the beam. This can be seen in Figure 3-4. The specimen was cycled to 2,000,000 cycles with insignificant damage accumulation. A tap test was done on the CFRP and several locally debonded zones were noted located as follows:

south of midspan	**north of midspan**
33.5” to 36” (851 mm to 914 mm)	7.5” to 8.75” (190 mm to 222 mm)
40.5” to 43” (1029 mm to 1092 mm)	25.75” to 26.75” (654 mm to 679 mm)
46.25” to 47.5” (1175 mm to 1207 mm)	55” to 56.5” (1397 mm to 1435 mm)
62.75” to 63.75” (1594 mm to 1619 mm)	60” to 61.5” (1524 mm to 1563 mm)

These debonded zones may have resulted from fatigue-induced damage although some are believed to be the result of poor application of the adhesive and the CFRP strip. The monotonic cycle resulted in significantly different load-deflection behavior than the companion Specimen L4. Specimen L4F had an ultimate load capacity of 11.54 kips (51.3 kN) and exhibited less ductility when compared to its companion Specimen L4. Debonding appeared to initiate at the toe of the shear crack and progress toward the south support. Complete debonding of the strip occurred from 3 in. (75 mm) north of midspan to the south support. The load vs. strain plot for Specimen L4F can be found in Figure 3-19.

3.2.5 Specimen H1F

The testing of Specimen H1F resulted in a fatigue-induced reinforcing bar rupture. The stiffness of Specimen H1F and companion Specimen H1 were nearly identical. This can be seen in Figure 3-5. The rupture of the east reinforcing bar became apparent after cycle 424,422. At this point, the stiffness of the beam changed significantly and an increase in midspan deflection was evident. There was also significant cracking near midspan due to the energy release associated with a fatigue rupture and increased beam deformation. The test was continued until cycle 597,445, at which time the remaining two reinforcing bars ruptured and the CFRP debonded. The failure mode of Specimen L1F was fatigue-induced reinforcing steel rupture.

3.2.6 Specimen H2F

The testing of Specimen H2F resulted in a fatigue-induced reinforcing bar rupture. The stiffness of Specimen H2F and companion Specimen H2 were nearly identical. This can be seen in Figure 3-6. The rupture of the east reinforcing bar became apparent after cycle 1,128,006. At this point, the stiffness of the beam changed significantly and an increase in midspan deflection was evident. The rupture was also evident from the behavior of the existing crack in the vicinity

of the rupture location. The width of the crack increased significantly following rupture of the reinforcing steel. The fatigue test was terminated following the reinforcing steel rupture. A tap test was performed on the CFRP to determine the extent of the debonding. Debonding was only found in the vicinity of the reinforcing bar rupture. This local debonding is believed to be attributed to damage caused by the energy release from the reinforcing bar rupture. The failure mode of Specimen H2F was fatigue-induced reinforcing steel rupture.

3.2.7 Specimen H2x1F

Specimen H2x1F sustained 2,000,000 cycles of fatigue loading, at which point fatigue testing was terminated and a final monotonic test was run to fail the beam. Specimen H2x1F was slightly less stiff than the companion Specimen H2x1. This can be seen in Figure 3-7. The specimen was cycled to 2,000,000 cycles during which some debonding resulted. The debonding is not evident from the strain data but it is apparent from the results of a tap test. By way of a tap test, significant debonding was noted from 8 to 15 in. (200 to 380 mm) north and south of midspan. Some debonding was also noted at midspan. Specimen H2x1F behaved very similar to the companion Specimen H2x1. A loss in ductility is the only difference noted from the load-deflection plot. The eventual failure mode was a splitting failure where the longitudinal steel and its concrete cover separate from the body of the beam, resulting in loss of all capacity; although debonding was evident before this failure occurred. Specimen H2x1F had an ultimate capacity of 10.19 kips (45.3 kN). The load vs. strain plot for Specimen H2x1F can be found in Figure 3-20.

3.2.8 Specimen H4F

Specimen H4F sustained 2,000,000 cycles of fatigue loading, at which point fatigue testing was terminated and a final monotonic test was run to fail the beam. Specimen H4F was slightly less stiff than the companion Specimen H4. This can be seen in Figure 3-8. Debonding

resulted from the fatigue loading. Based on strain data, the debonding was noted at the locations of gages 2 and 6 at approximately N = 120,000 cycles and was apparent from the results of a tap test. This can be seen in Figure 3-17b. Debonding was noted from 7 to 11 in. (175 to 275 mm) north of midspan across the whole width of the CFRP. Following the monotonic cycle, complete debonding was apparent from 15 in. (380 mm) north of midspan to the south support. Specimen H4F had an ultimate capacity of 12.1 kips (53.8 kN). The load vs. strain plot for Specimen H4F can be found in Figure 3-21.

Table 3-1 Summary of key parameters and test results from fatigue tests.

		CF	L1F	L2F	L2X1F	L4F	H1F	H2F	H2X1F	H4F
b_f/b		na	0.167	0.333	0.333	0.667	0.167	0.333	0.333	0.667
adhesive type		na	SikaDur 23				SikaDur 30			
age at start of fatigue test	days	175	184	191	231	274	210	217	238	253
cracking load	kips	0.68	0.66	0.68	0.69	0.67	0.67	0.67	0.69	0.73
cracking moment	kip-in	30	29	30	31	30	30	30	31	32
N = 2										
minimum applied load	kips	1.01	1.04	1.03	1.02	1.04	1.02	1.03	1.04	1.01
minimum applied moment	kip-in	45	46	46	46	46	45	46	46	45
deflection at minimum applied load	in	0.29	0.27	0.26	0.29	0.22	0.32	0.29	0.27	0.21
maximum rebar strain at minimum applied load	με	747	717	633	622	523	700	610	633	474
maximum FRP strain at minimum applied load	με	na	647	663	640	548	815	787	806	506
maximum applied load	kips	4.98	5.00	5.00	5.00	5.00	4.99	5.00	5.00	5.00
maximum applied moment	kip-in	222	223	223	223	223	223	223	223	223
deflection at maximum applied load	in	0.78	0.76	0.67	0.74	0.59	0.81	0.75	0.70	0.62
maximum rebar strain at maximum applied load	με	1950	1954	1668	1658	1393	1895	1606	1734	1351
maximum FRP strain at maximum applied load	με	na	1869	1758	1778	1479	2127	1997	2089	1428
range of applied load	kips	3.98	3.96	3.98	3.98	3.96	3.98	3.97	3.96	3.99
range of applied moment	kip-in	178	177	178	178	177	178	177	177	178
stress range in rebar	ksi	34.9	35.9	30.0	30.0	25.2	34.7	28.9	31.9	25.4
stress range in FRP	ksi	na	27.5	24.6	25.6	20.9	29.5	27.2	28.9	20.7
secant stiffness	kip/in	7.92	7.85	9.36	8.72	10.59	8.09	8.38	9.19	9.53
last recorded cycle before failure (N_f)		>329324[1]	400867	2000000	447695	2000000	424422	1128006	2000000	2000000
failure mode during fatigue cycling		na	FIRR[2]	run-out	FIRR[2]	run-out	FIRR[2]	FIRR[2]	run-out	run-out
N = N_f, or N = 2000000										
minimum applied load	kips	na	1.12	1.00	1.02	1.00	1.02	1.01	1.00	1.00
minimum applied moment	kip-in	na	50	45	45	45	46	45	45	45
deflection at minimum applied load	in	na	0.36	0.27	0.32	0.29	0.42	0.36	0.33	0.30

Table 3-1 (continued)

		CF	L1F	L2F	L2X1F	L4F	H1F	H2F	H2X1F	H4F
maximum rebar strain at minimum applied load	με	na	679	607	641	508	714	598	628	527
maximum FRP strain at minimum applied load	με	na	659	638	611	518	912	832	837	556
maximum applied load	kips	na	5.00	5.00	5.00	5.00	5.00	5.00	5.00	5.00
maximum applied moment	kip-in	na	223	223	223	223	223	223	223	223
deflection at maximum applied load	in	na	0.88	0.79	0.81	0.74	0.95	0.87	0.84	0.77
maximum rebar strain at maximum applied load	με	na	1832	1809	1790	1511	1962	1684	1881	1505
maximum FRP strain at maximum applied load	με	na	1980	1864	1819	1545	2327	2158	2279	1638
range of applied load	kips	na	3.88	4.00	3.98	4.00	3.98	3.99	4.00	4.00
range of applied moment	kip-in	na	173	179	178	179	178	178	179	179
stress range in rebar	ksi	na	33.4	34.9	33.3	29.1	36.2	31.5	36.3	28.4
stress range in FRP	ksi	na	29.7	27.6	27.2	23.1	31.8	29.8	32.4	24.3
secant stiffness	kip/in	na	7.29	7.69	8.07	8.64	7.43	7.86	7.58	8.37

[1]Specimen loaded to failure due to equipment malfunction
[2]FIRR = fatigue-induced reinforcing bar rupture

any N										
maximum observed strain in FRP	με	na	1988	1873	1819	1545	2327	2158	2285	1638
corresponding rebar strain	με	na	1792[4]	1809	1658	1511[3]	1962[3]	1684	1526	1263
cycle number		na	342629	1698454	447695	2000000	424422	1128006	1820072	2000000
strain in FRP at initiation of debonding	με	na	[5]	[6]	[5]	[6]	n.o.	[5]	[6]	1565
corresponding rebar strain	με	na	[5]	[6]	[5]	[6]	n.o.	[5]	[6]	1552
cycle number		na	[5]	[6]	[5]	[6]	n.o.	[5]	[6]	118213

[3]strain gage #2 was lost so gage #3 was reported
[4]strain gage #3 was lost so gage #2 was reported
[5]debonding observed in vicinity of FIRR only
[6]debonding observed but not propagating beyond strain gage location
n.o. = not observed

Table 3-2 Summary of key parameters and test results from run-out monotonic tests.

		L2F	**L4F**	**H2x1F**	**H4F**
b_f/b		0.333	0.667	0.333	0.667
adhesive type		SikaDur 23		SikaDur 30	
age at start of fatigue test	days	191	274	238	253
cracking load	kips	0.68	0.67	0.69	0.73
cracking moment	kip-in	30	30	31	32
load at initial yield of reinforcing	kips	6.15	7.51	5.85	7.61
moment at initial yield of reinforcing	kip-in	275	335	261	340
deflection at initial yield of reinforcing	in	0.92	1.03	0.94	1.06
load at general yield	kips	8.88	10.66	9.49	11.43
moment at general yield	kip-in	397	476	424	510
deflection at general yield	in	1.29	1.42	1.39	1.59
maximum load	kips	10.23	11.54	10.19	12.10
maximum moment	kip-in	457	515	455	540
deflection at max load	in	2.30	1.97	1.89	1.98
deflection at ultimate load (80% max)	in	2.65	2.38	2.02	2.07
displacement ductility		2.06	1.68	1.45	1.30
maximum observed strain in FRP	με	7444	5807	6970	5860
corresponding rebar strain	με	3238	9916	13039	10885
maximum strain in FRP at time of max load	με	7322	5180	6875	5860
corresponding rebar strain	με	4171	9897	13664	10885
strain in FRP at initiation of debonding	με	4301	3854	3909	3260
corresponding rebar strain	με	2898	2706	2767	2767

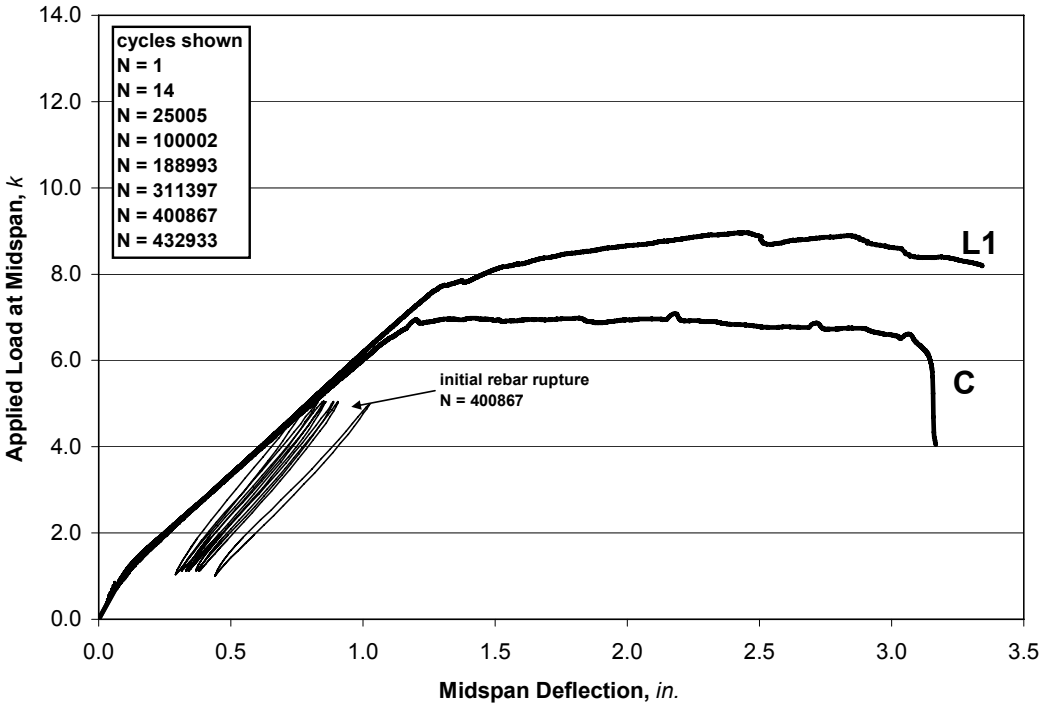

Figure 3-1 Load-deflection behavior for Specimen L1F for various cycles of loading.

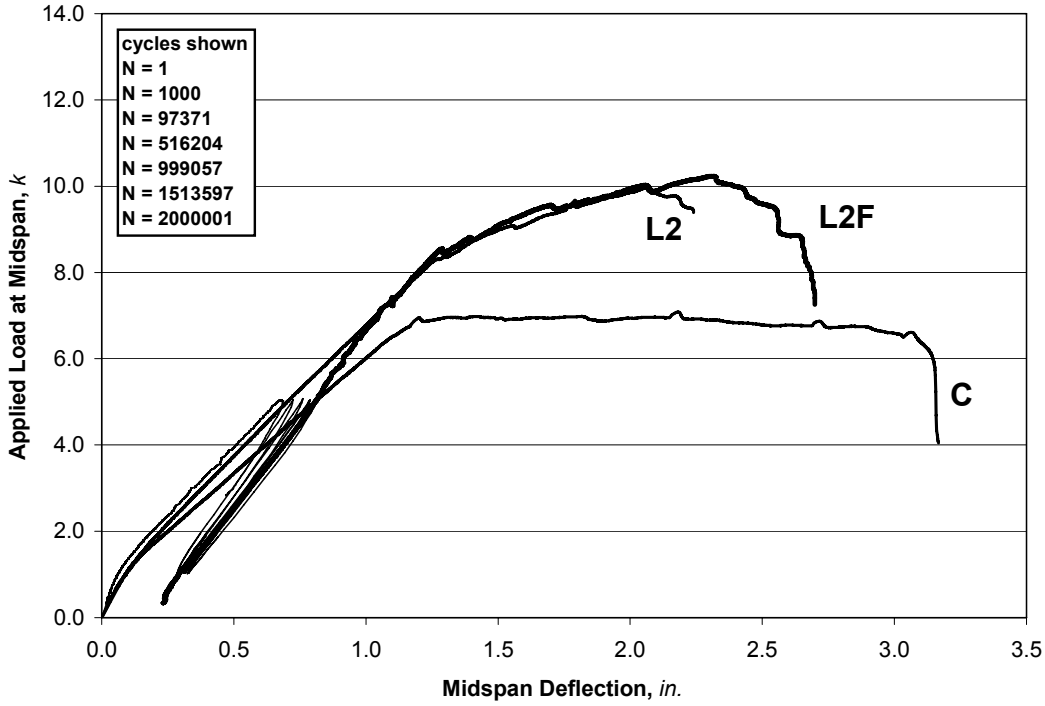

Figure 3-2 Load-deflection behavior for Specimen L2F for various cycles of loading.

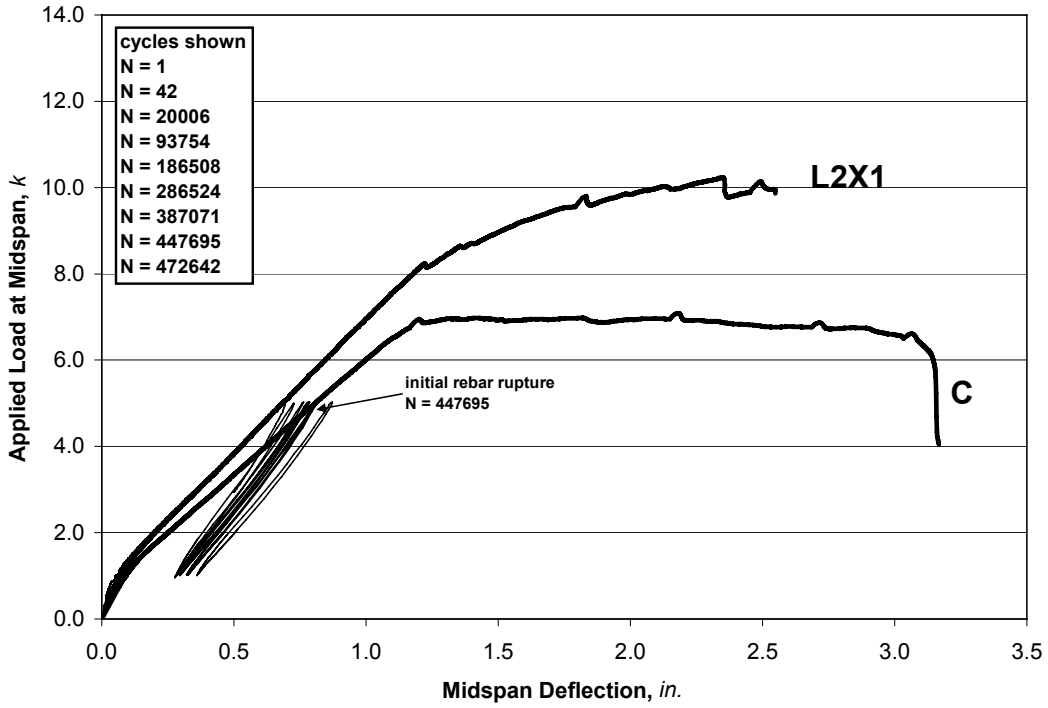

Figure 3-3 Load-deflection behavior for Specimen L2x1F for various cycles of loading.

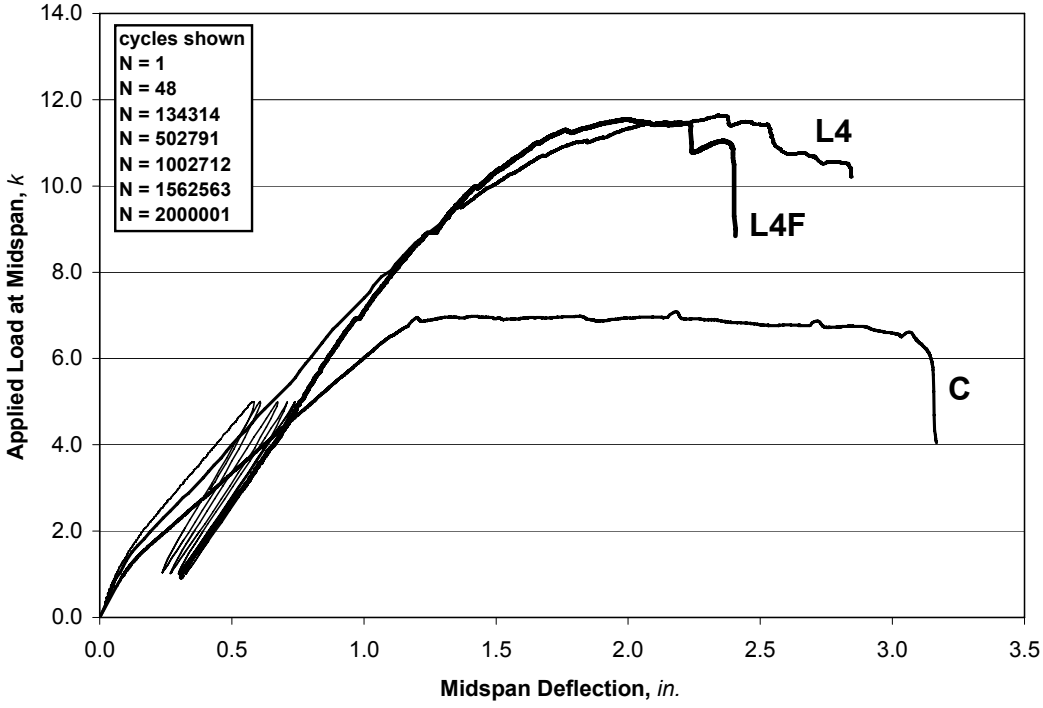

Figure 3-4 Load-deflection behavior for Specimen L4F for various cycles of loading.

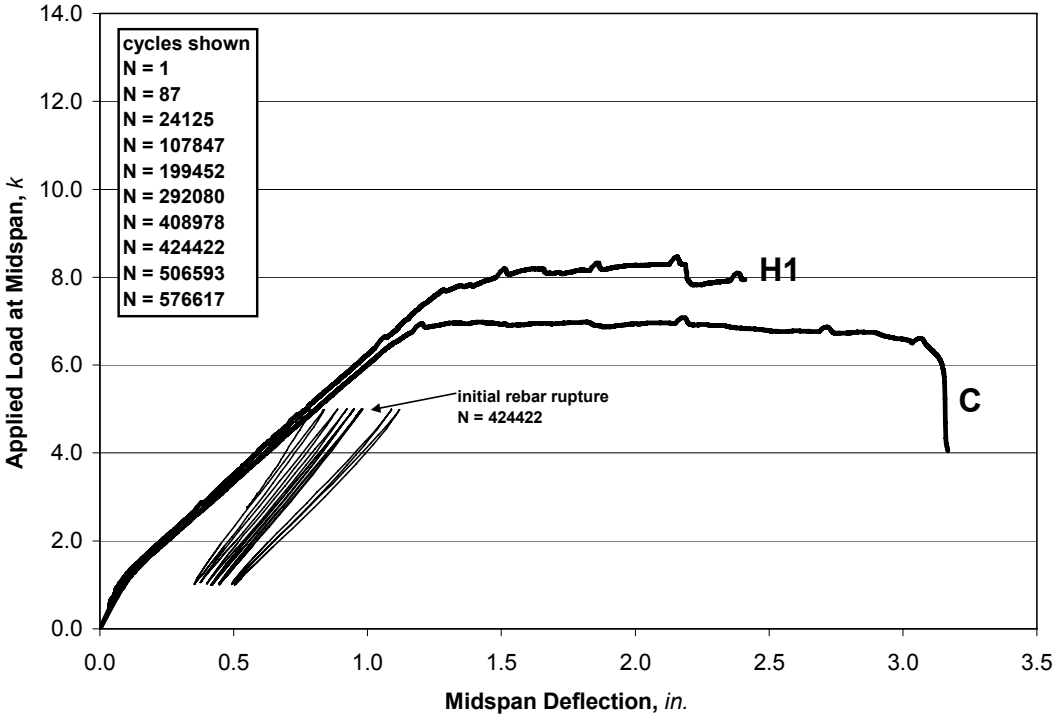

Figure 3-5 Load-deflection behavior for Specimen H1F for various cycles of loading.

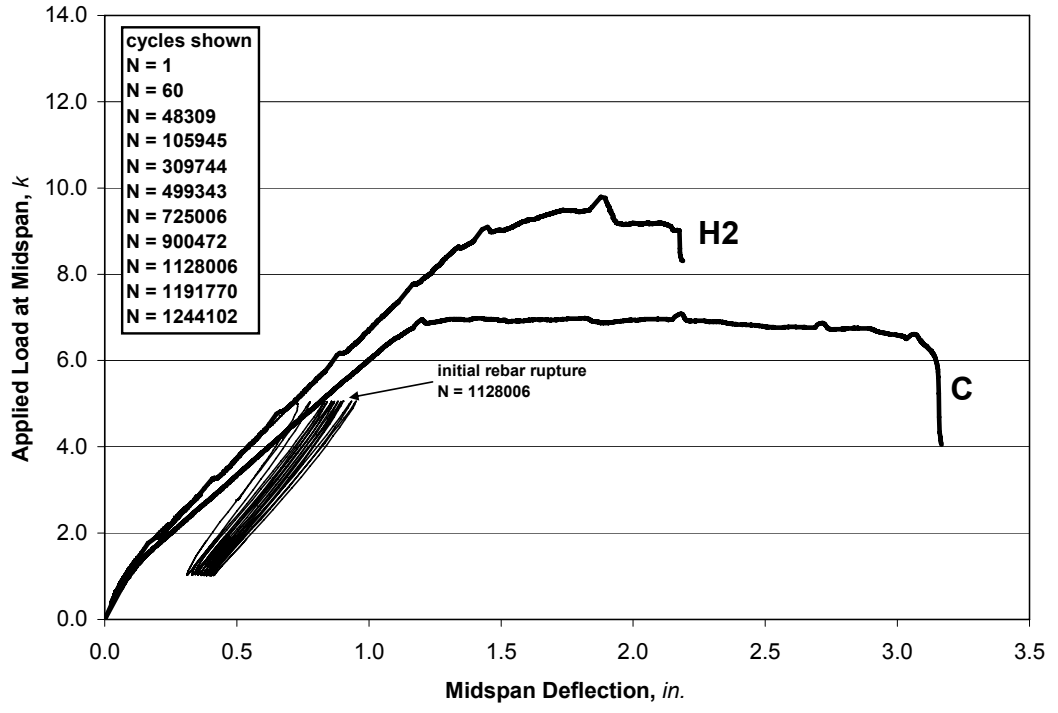

Figure 3-6 Load-deflection behavior for Specimen H2F for various cycles of loading.

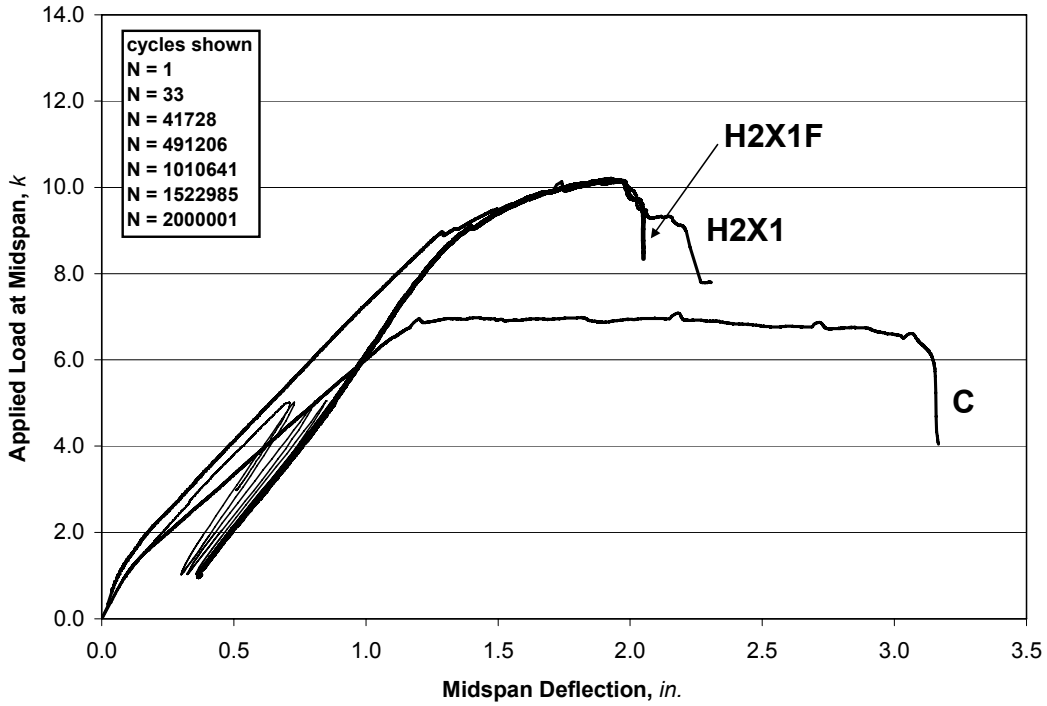

Figure 3-7 Load-deflection behavior for Specimen H2x1F for various cycles of loading.

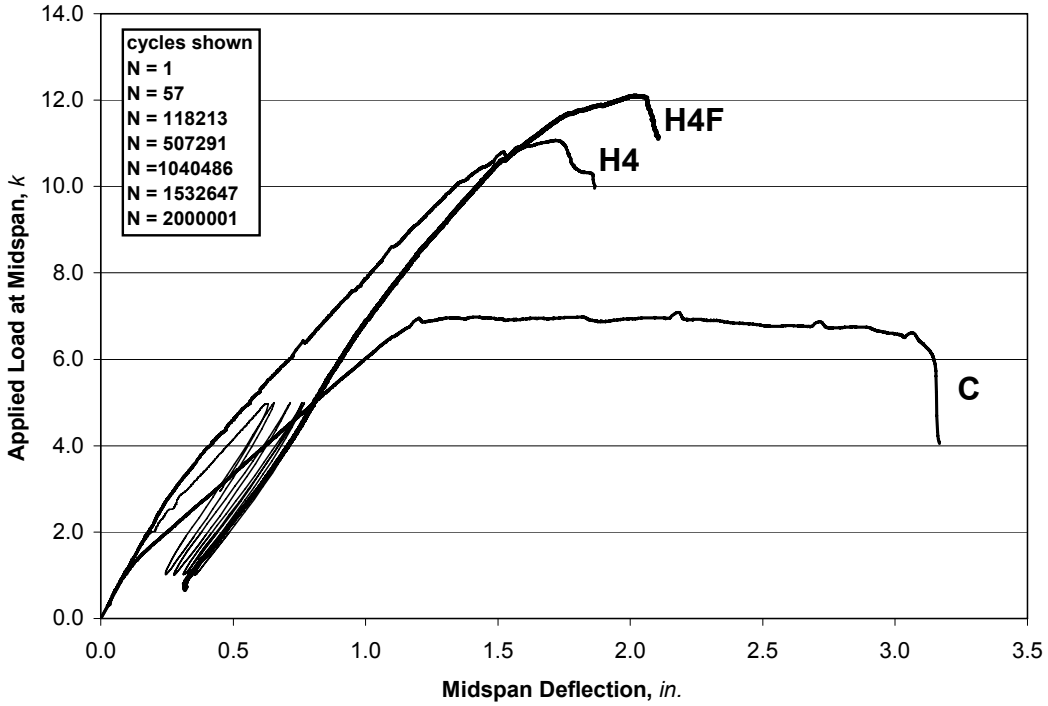

Figure 3-8 Load-deflection behavior for Specimen H4F for various cycles of loading.

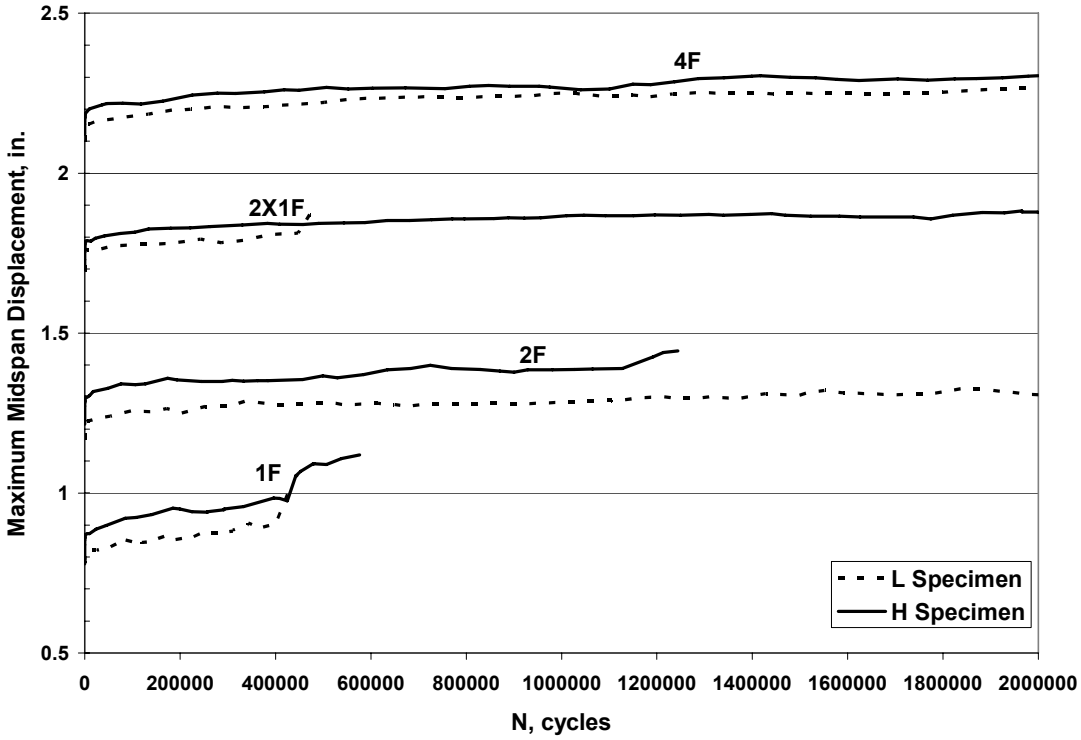

Figure 3-9 Midspan deflection accumulation curves for all eight specimens (curve pairs shifted vertically 0.5 inches for clarity).

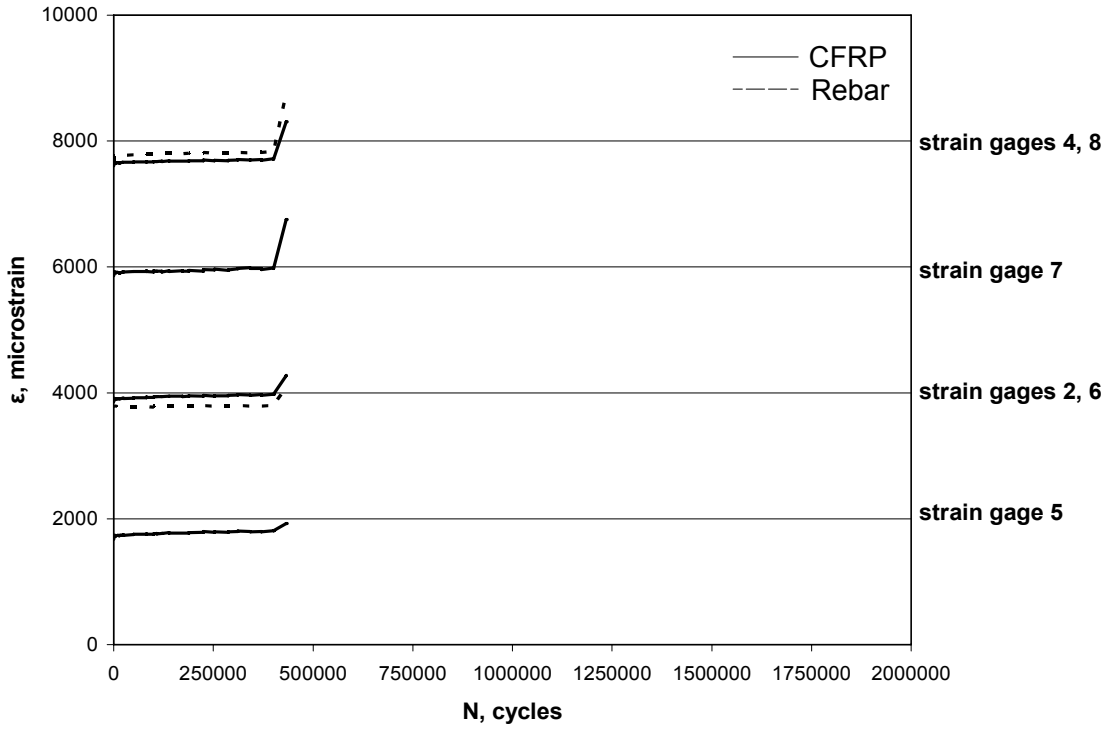

Figure 3-10 Strain accumulation curves for Specimen L1F (shifted vertically 2000 με).

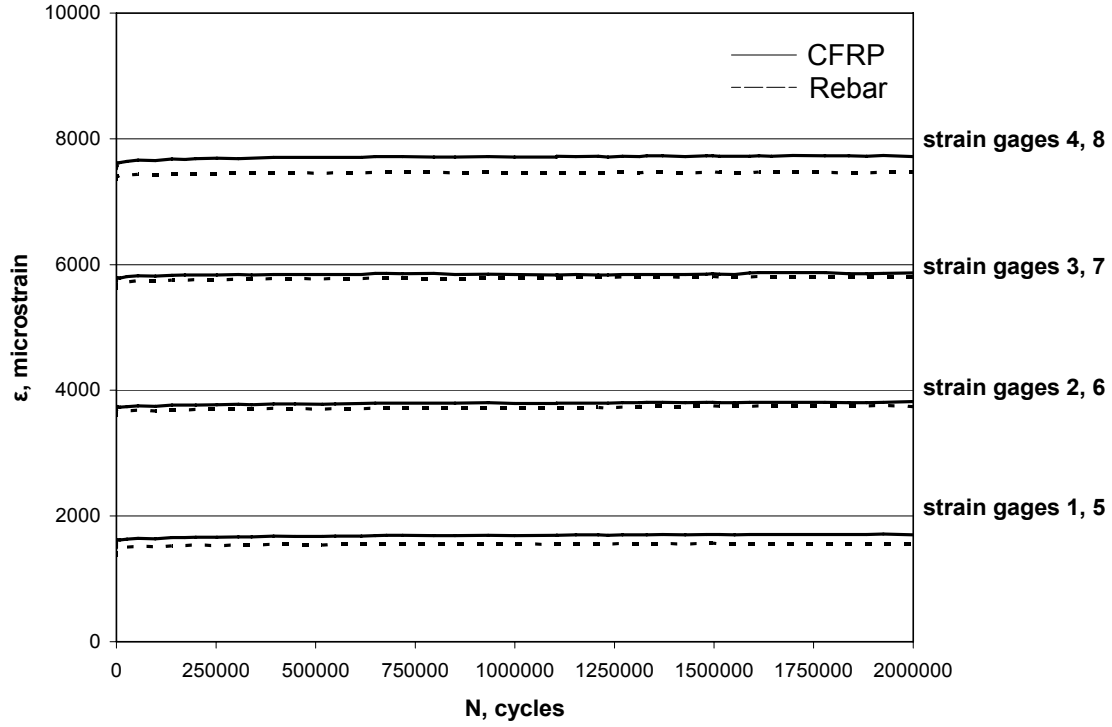

Figure 3-11 Strain accumulation curves for Specimen L2F (shifted vertically 2000 με).

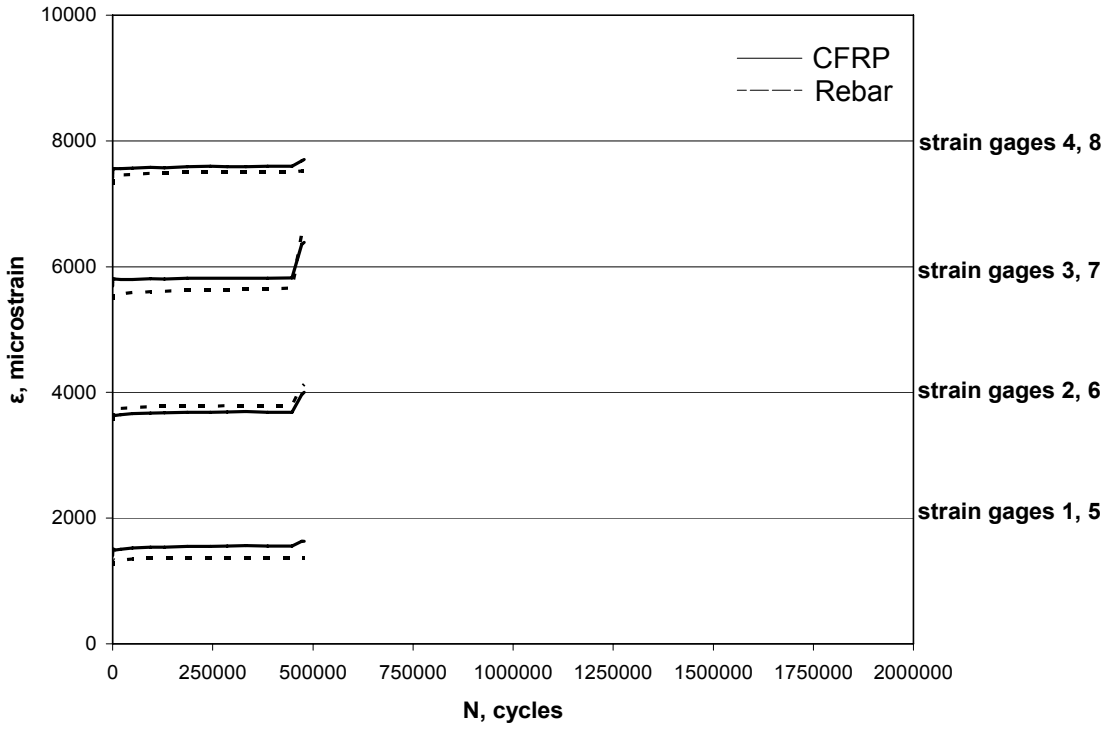

Figure 3-12 Strain accumulation curves for Specimen L2x1F (shifted 2000 με).

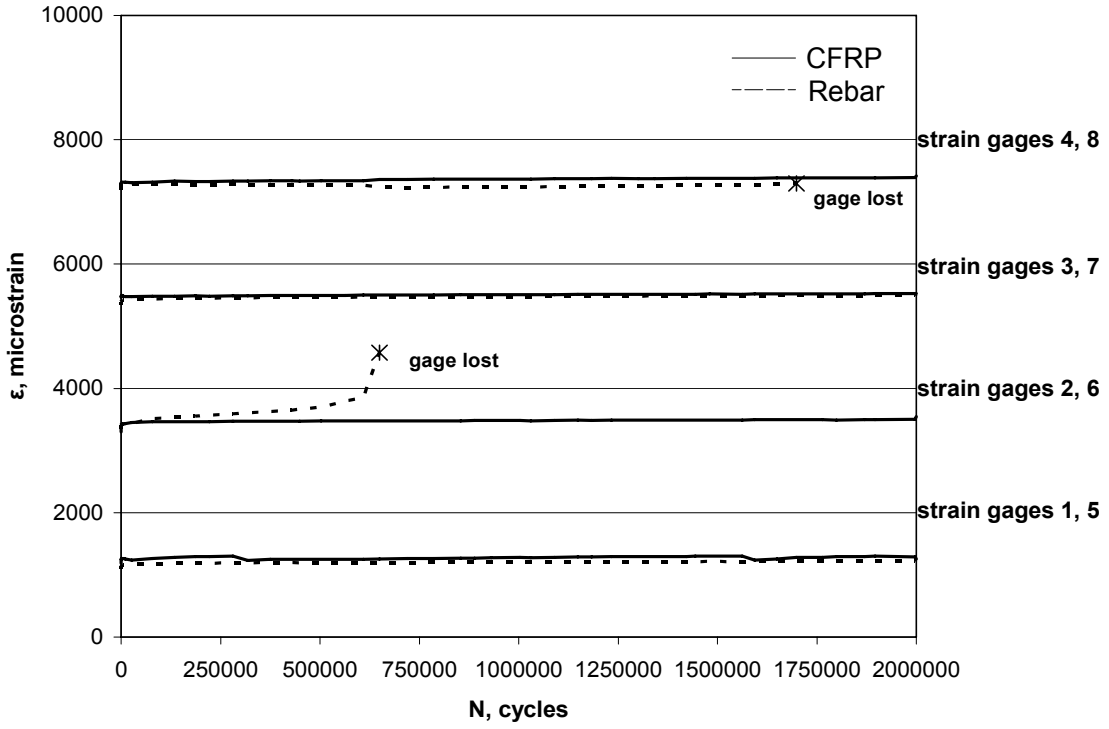

Figure 3-13 Strain accumulation curves for Specimen L4F (shifted vertically 2000 με).

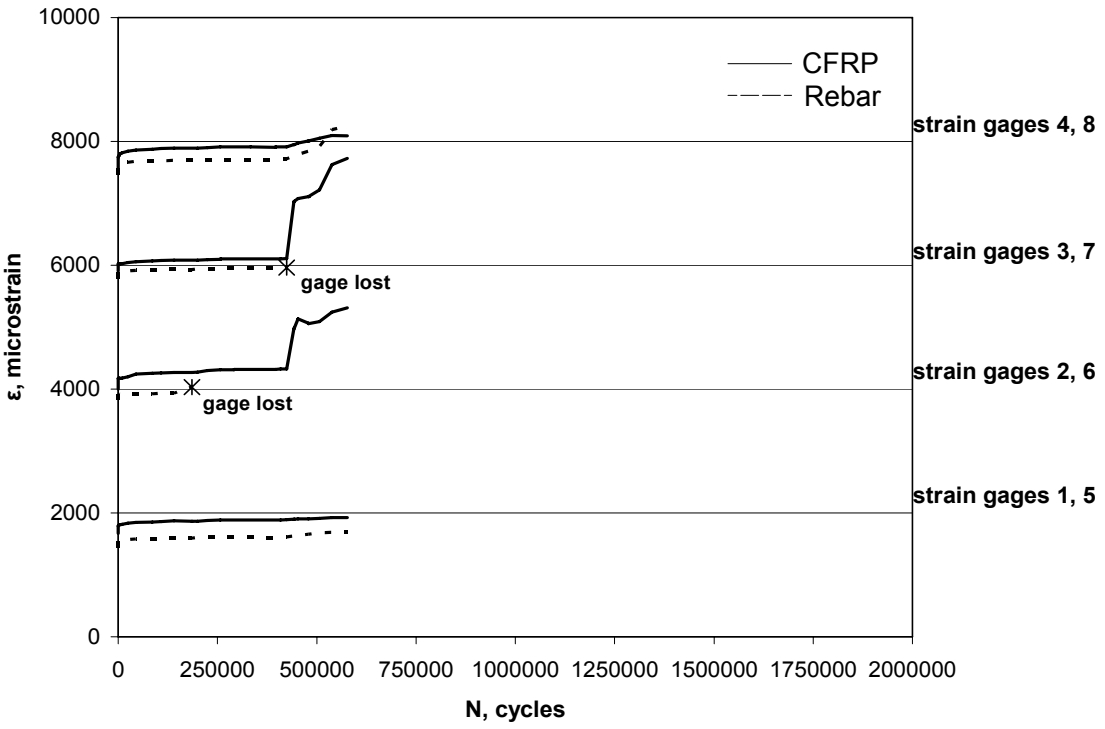

Figure 3-14 Strain accumulation curves for Specimen H1F (shifted vertically 2000 με).

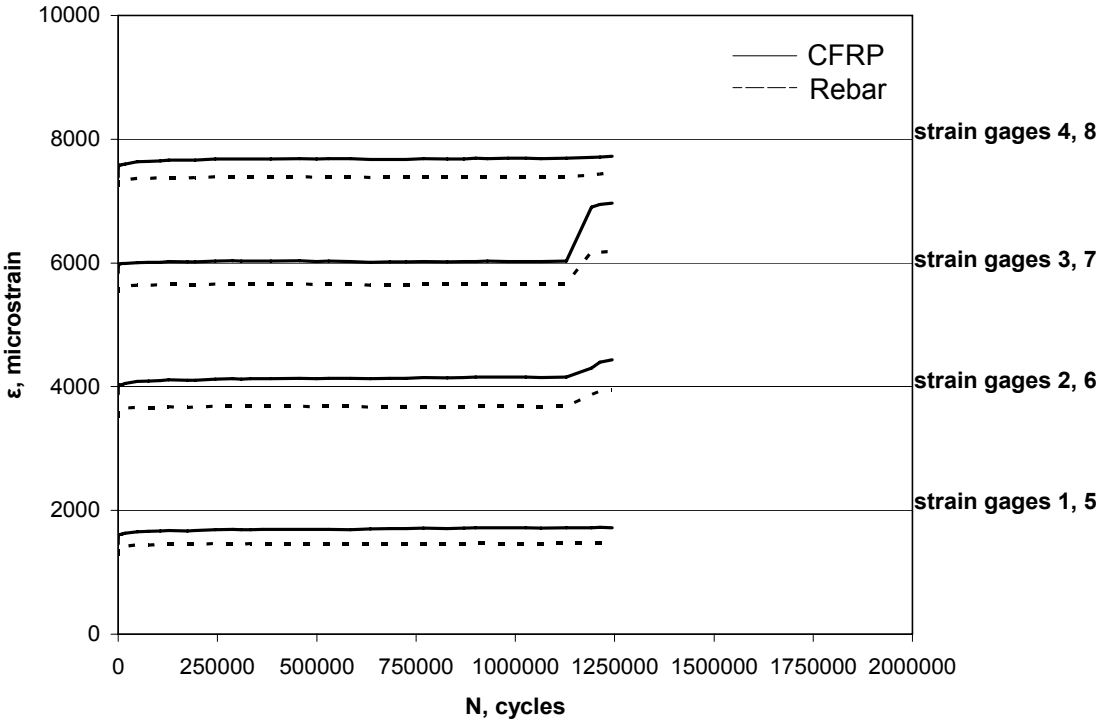

Figure 3-15 Strain accumulation curves for Specimen H2F (shifted vertically 2000 με).

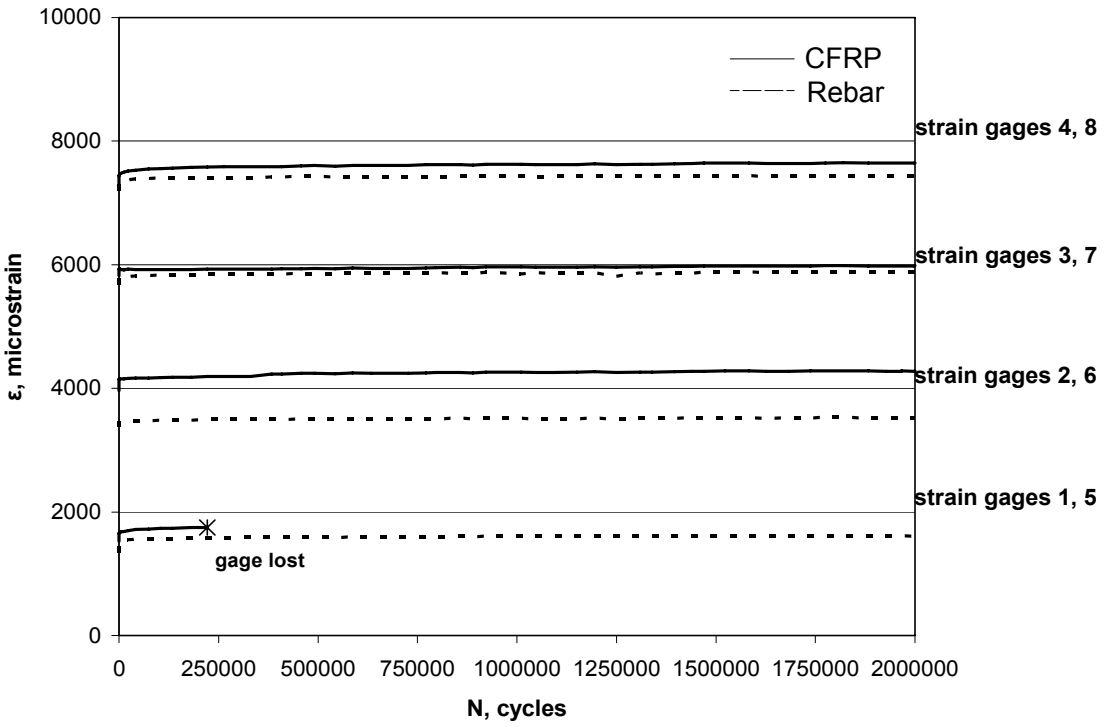

Figure 3-16 Strain accumulation curves for Specimen H2x1F (shifted 2000 με).

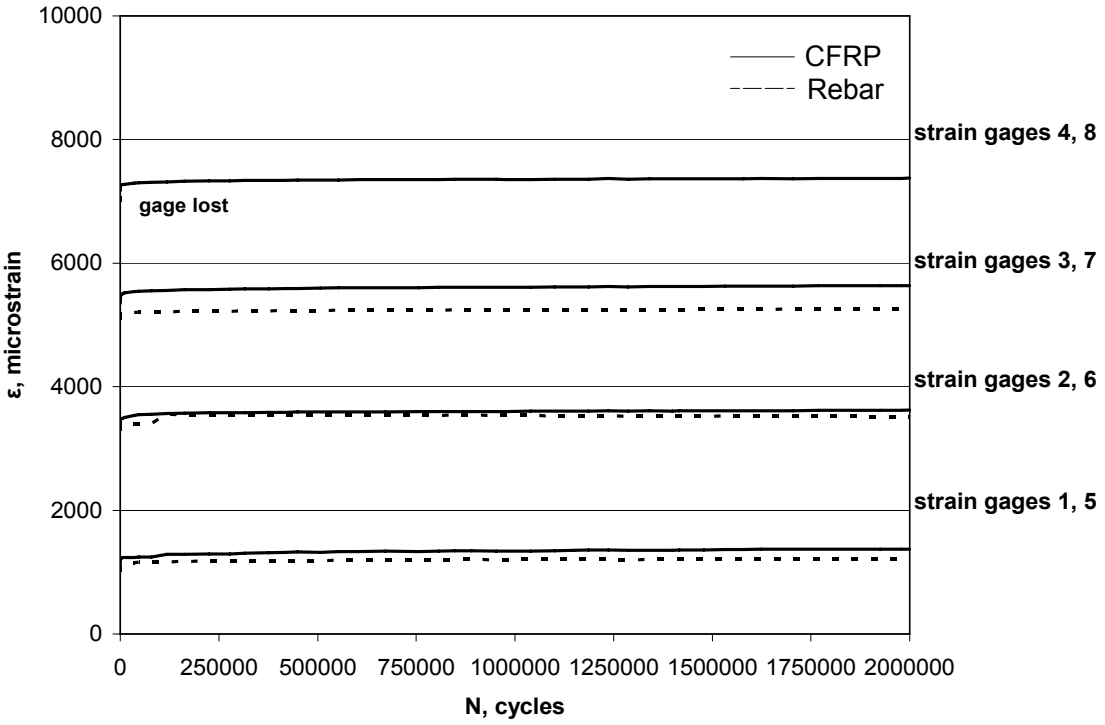

Figure 3-17a Strain accumulation curves for Specimen H4F (shifted vertically 2000 με).

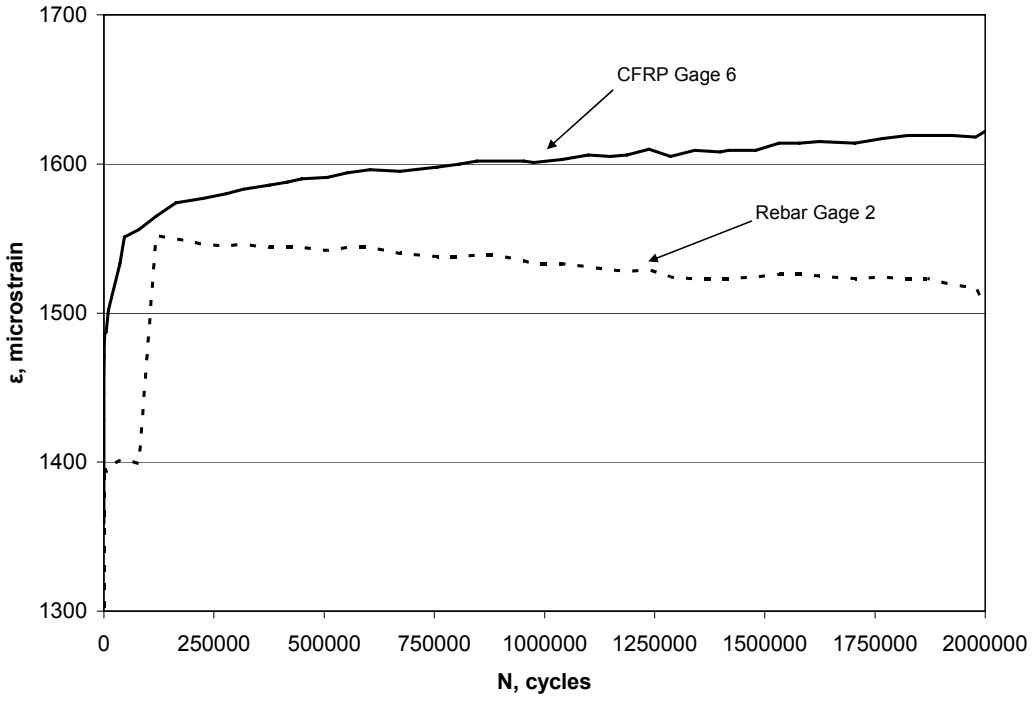

Figure 3-17b Strain accumulation curves for Specimen H4F (Gages 2 and 6, no vertical shift)

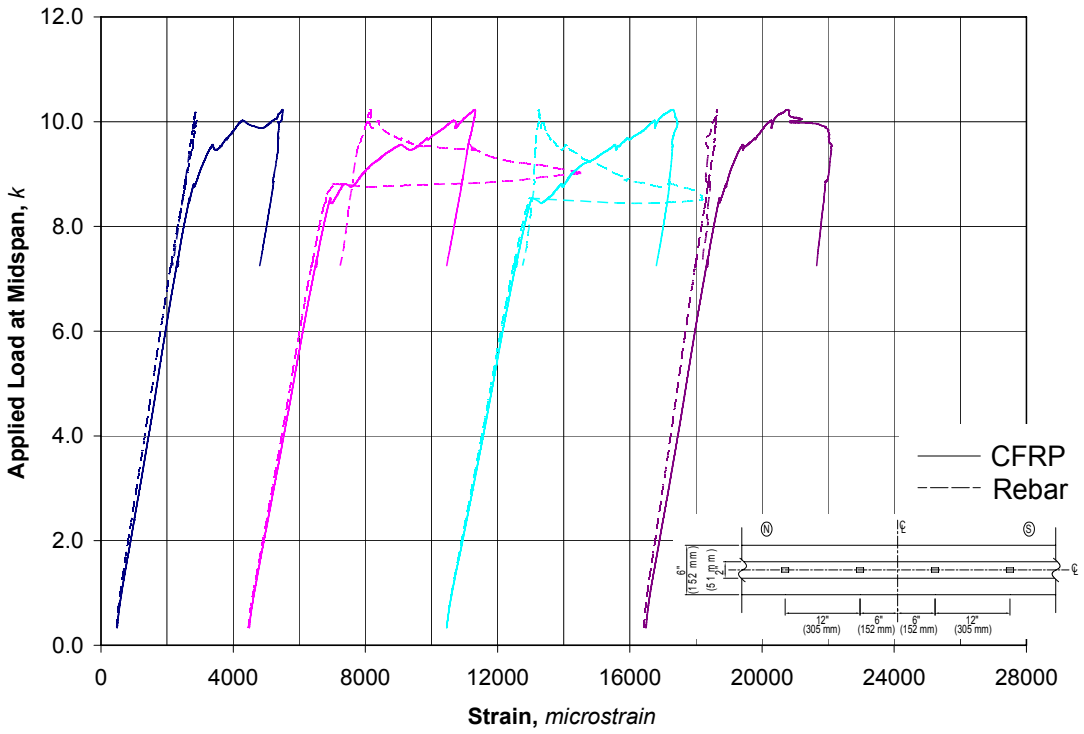

Figure 3-18 Load-strain behavior of Specimen L2F (shifted horizontally 4000 με).

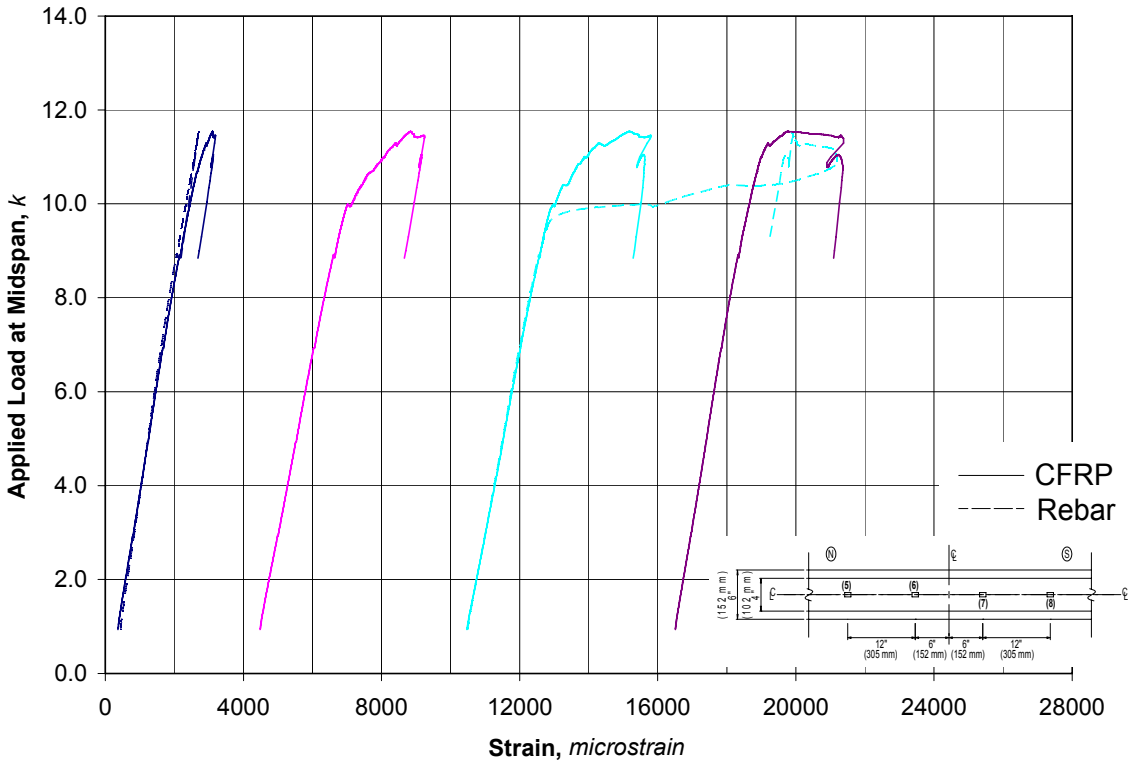

Figure 3-19 Load-strain behavior of Specimen L4F (shifted horizontally 4000 με).

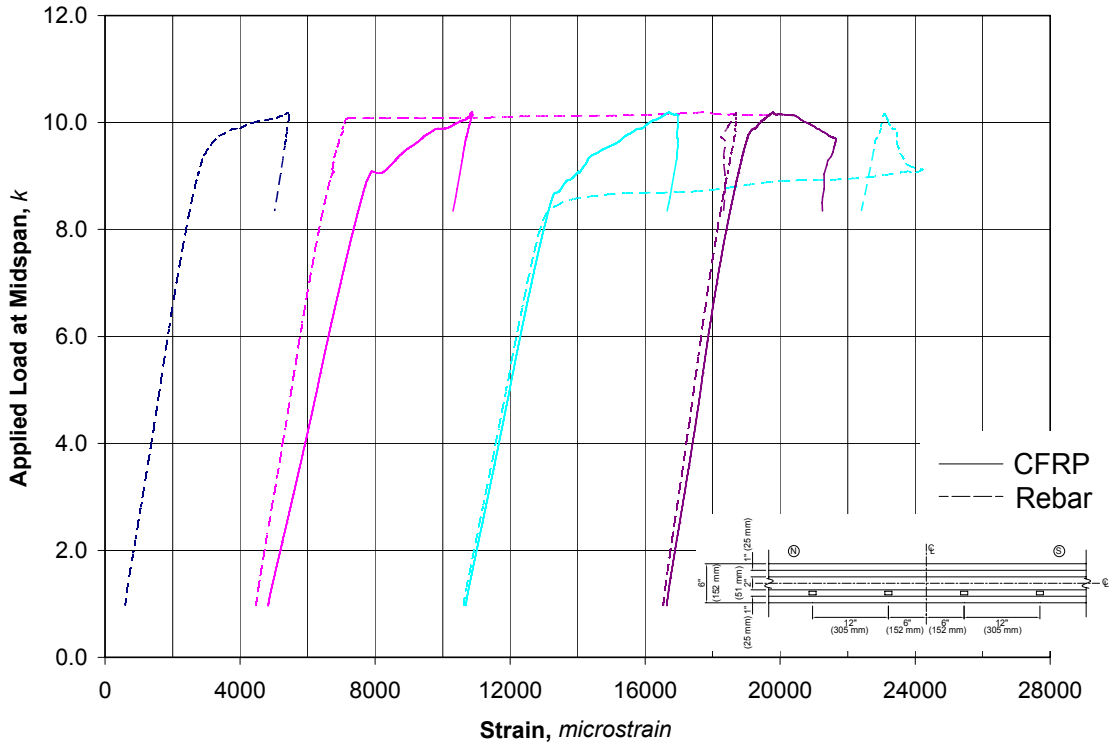

Figure 3-20 Load-strain behavior of Specimen H2x1F (shifted horizontally 4000 με).

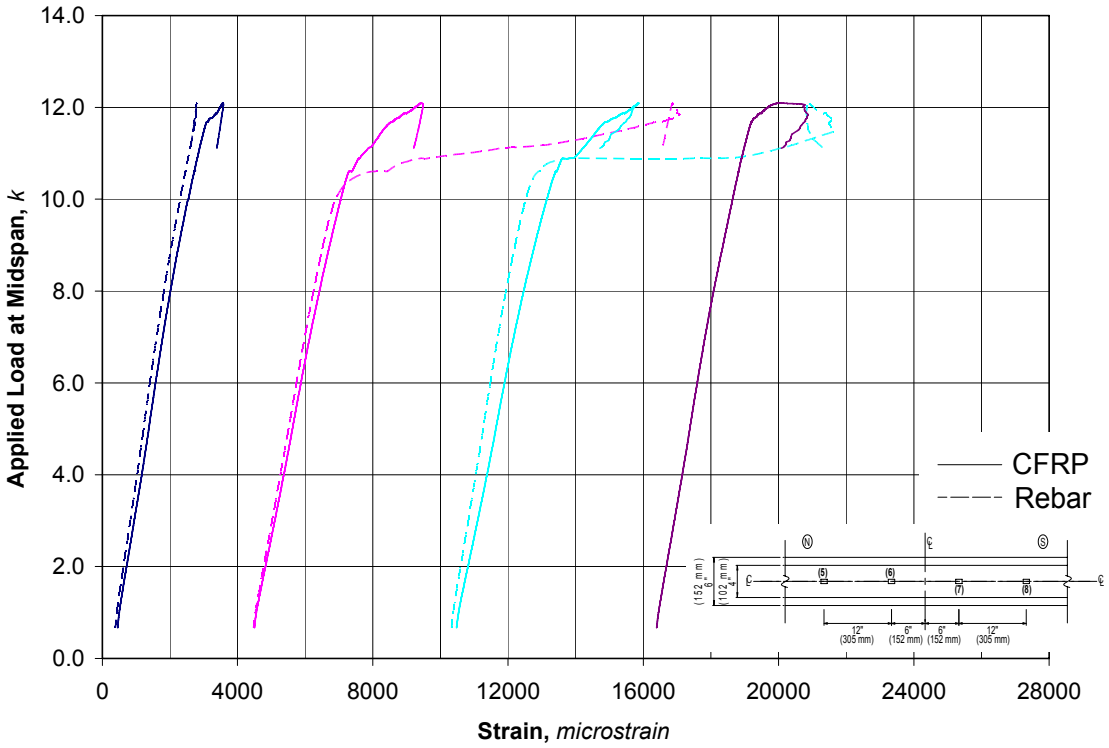

Figure 3-21 Load-strain behavior of Specimen H4F (shifted horizontally 4000 με).

Figure 3-22 Typical fatigue-induced reinforcing bar rupture

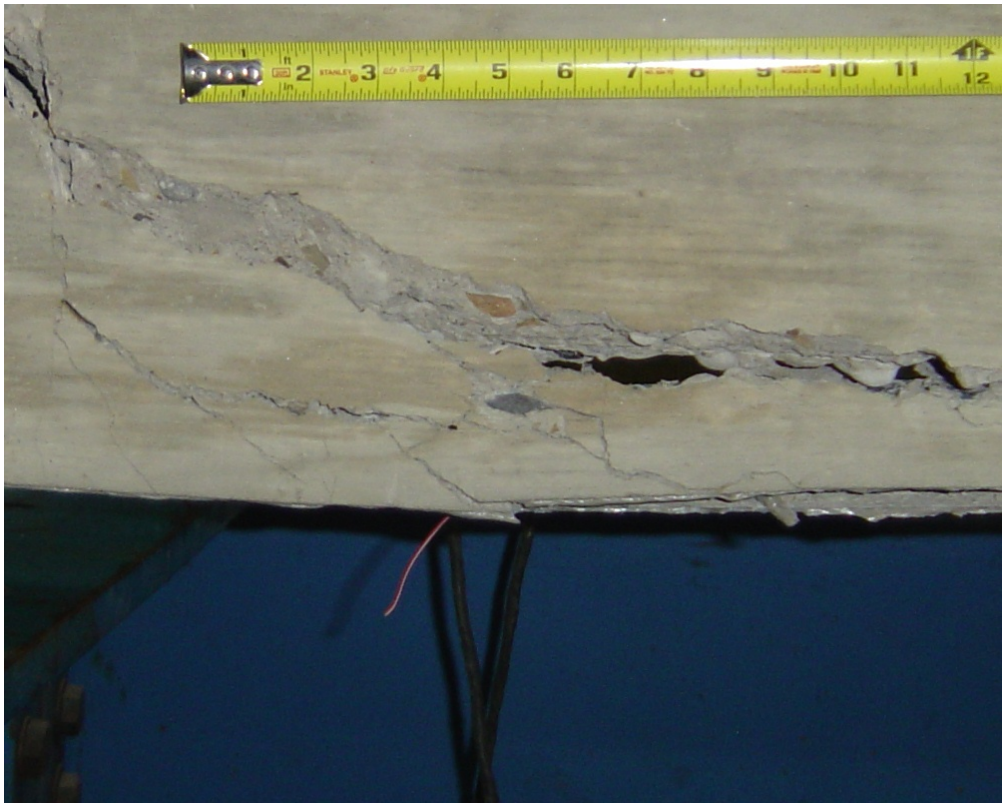

Figure 3-23 Representative debonding at toe of shear crack. (Splitting failure is secondary.)

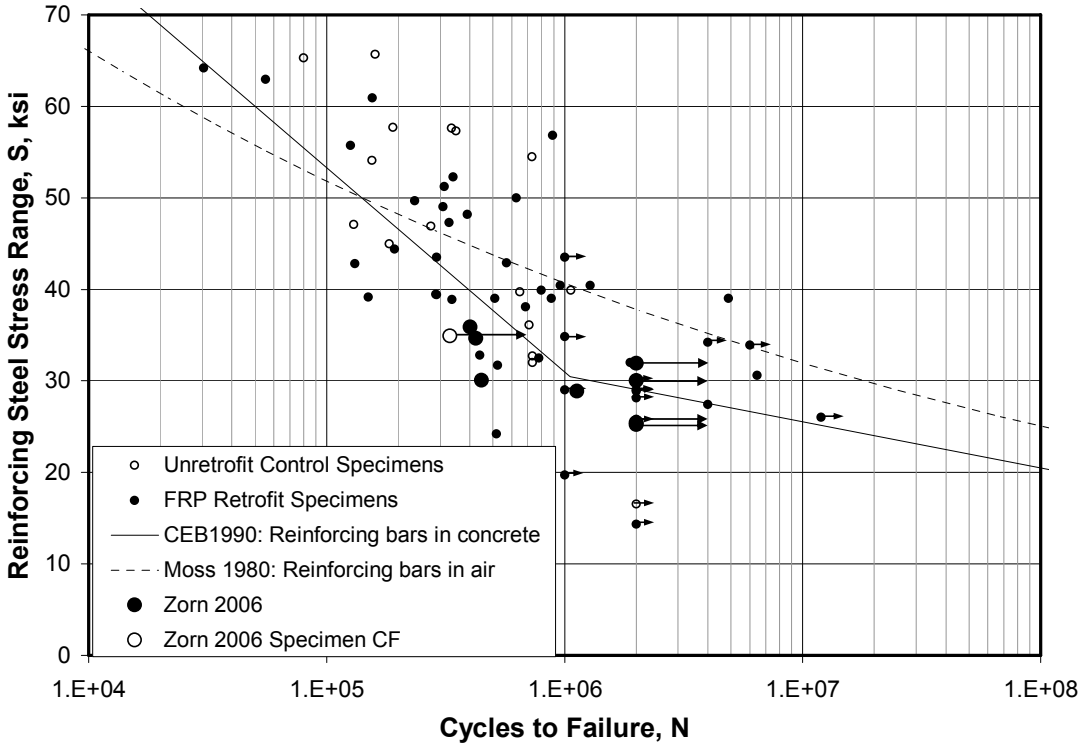

Figure 3-24 SN Curve of all existing data including those tested in this program.

4.0 DISCUSSION OF EXPERIMENTAL RESULTS

This chapter reports interpretations of and results derived from the experimental data reported in Chapter 3. Basis for these interpretations is also reported.

4.1 COMPARISON OF FATIGUE TESTS SPECIMENS

Both the fatigue failure and fatigue run-out specimens are reported in the following sections. The CFRP applications have been normalized in the following manner:

$$equivalent\ reinforcement\ ratio = \frac{A_s}{bh} + \frac{A_f}{bh}\frac{E_f}{E_s} \tag{4-1}$$

Where A_s is the area of steel reinforcement; A_f is the area of CFRP; E_f/E_s is the modular ratio of CFRP to steel and bh is the gross concrete section area. In all cases reported A_s/bh = 0.01. Material properties and dimensions are reported in Chapter 2. The added CFRP increases the equivalent reinforcement ratio only modestly – to a maximum of 0.0128 in the case of the 4-series specimens.

The S-N data reported in Table 3-1 is plotted in Figure 4-1 along with representative S-N relationships (Moss 1980 and CEB 1990, as discussed in Chapter 1). The four run-out specimens are noted with arrows and the four specimens exhibiting fatigue-induced reinforcing bar rupture are duly noted. The control fatigue specimen, CF, which was inadvertently loaded to failure during an equipment malfunction, is noted as an open circle with an arrow signifying that the actual fatigue life was greater than the last cycle recorded.

Although the stress ranges reported in this study are relatively similar, the fatigue lives vary considerably (i.e.: the S-N data is relatively "flat"). This is an indication of the sensitivity of

the behavior of the bonded systems tested and of the fact that the stress ranges used were close to the expected endurance limit for the reinforcing bar material. Additionally, it appears that the present data (solid circles in Figure 4-1) falls somewhat "below" other comparable data, although generally within the expected scatter for fatigue data.

4.1.1 Stress Range "Drift"

It is critical to note that S-N data is traditionally based on the stress range determined at the initial cycle (N =1). In the present study, N = 2 is used since N = 1 was used to crack the concrete beam and has somewhat different response. Nonetheless, the stress range in the reinforcing steel is expected to increase with cycling. This increase or "drift" may be attributed to the following:

1. Softening of concrete under repeated compression loads, as described in Section 1.4.2 in relation to Heffernan (1997); and,
2. Degradation of the CFRP-to-concrete bond resulting in more stress being carried by the reinforcing steel.

In the tests reported, the stress range in the reinforcing steel increases between 4% and 16% from N = 2 to N = N_f as reported in Table 4-1. Only Specimen L1F has an apparent decrease in the value of S, although this may be attributed to a higher minimum stress being recorded in the final instrumented cycle at N = 400,867 as shown in Table 3-1. Figure 4-1 shows the effects of the stress range drift in relation to the S-N data presented. As can be seen, if the value of S determined at N_f (solid diamond shaped data points) is used, the S-N results are shifted upwards. This shift is proportional to the fatigue life and is generally unaffected by other parameters investigated.

4.1.2 Secant Stiffness

A similar measure of degradation due to fatigue cycling is the secant stiffness; defined as the slope of the load-deflection relationship obtained during cycling. As can be seen in Table 4-1, this degradation is consistent for all specimens, with the final secant stiffness ($N = N_f$) ranging from 82% to 94% of the ***cracked*** secant stiffness determined at N = 2. Like the stress range drift, the rate of degradation of this stiffness is also relatively consistent across all specimens. The cycle stiffness values, normalized by that determined at N = 2, are shown in Figure 4-2. In this figure it is relatively clear that degradation of the beam behavior (as measured by stiffness) is relatively constant regardless of the CFRP detail or adhesive property. This behavior is also not apparently affected by the initial stiffness which is observed to increase with an equivalent reinforcing ratio (see Table 3-1).

4.1.3 Retrofit Geometry

The amount of material used in a CFRP retrofit has a significant effect on the stress carried by the steel. Figure 4-3 shows the ratio of steel reinforcement stress at cycle N=2 to the steel reinforcement stress of the control fatigue specimen CF at cycle N=2. This comparison illustrates that at the fatigue loads considered (which may be interpreted as service loads), the relationship between the amount of CFRP reinforcement and the corresponding steel reinforcement stresses is an inverse linear relationship. This observed behavior is expected and is consistent with elastic beam theory. At ultimate load conditions, when concrete and steel behavior is no longer linear, the continued addition of CFRP material (i.e.: increasing the equivalent reinforcing ratio) has an incrementally reduced effect on load carrying capacity; that is there is a "law of diminishing returns" with respect to added CFRP (Reeve 2005). At the lower fatigue/service load levels considered, such an effect is not observed and the rate of improved

performance change is proportional to the increasing CFRP area provided. Additionally, at these lower fatigue/service load levels no discernable difference between specimens having high and low modulus adhesives was observed. Unfortunately, a comparison between the steel stresses at cycle $N=N_f$ to the steel stresses at cycle $N=N_f$ for the control specimen can not be made due to the loss of the control specimen before fatigue rupture of the steel reinforcement occurred. Nonetheless, the previous observation of similar stiffness degradation for all specimens suggests that a similar performance at N_f as at N = 2 will be observed.

4.2 COMPARISON OF FATIGUE RUN-OUT SPECIMENS

The following sections report the fatigue run-out specimens and their respective companion control specimens reported by Reeve (2005). In the interest of completeness, a summary of key behavioral data of Reeve's specimens – similar to that provided in Table 3-2 for the present specimens – is provided in Appendix A.

4.2.1 Effect of Fatigue Cycling on Debonding Strain

As described in Section 2.7.2, the fatigue run-out specimens sustained 2,000,000 cycles of fatigue loading and were then monotonically pushed to failure. Thus, these specimens are said to be "fatigue conditioned" prior to their final monotonic test. Changes in behavior were noted as compared to the monotonic control specimens reported by Reeve and attributed to the 2,000,000 cycles of fatigue conditioning.

Debonding strain was affected significantly by the cyclic loading, particularly for the L specimens. Strain at the initiation of debonding was recorded and plotted versus the equivalent reinforcement ratio for the four run-out specimens in Figure 4-4. Reeve (2005) notes that the debonding strains observed for the monotonically loaded L specimens (lower modulus adhesive) were significantly greater than those for the H specimens (higher modulus adhesive). This is

shown in Figure 4-4 as the open data points. The fatigue conditioned HF specimens, H2x1F and H4F; both exhibited debonding strains similar to their companion control specimens, H2x1 and H4. Debonding strains of the H specimens were not apparently affected by the fatigue conditioning. After fatigue conditioning, the LF specimens exhibited debonding strains similar to that of the H and HF specimens. The superior behavior of softer adhesive (L) is significantly less pronounced following fatigue conditioning (LF).

4.2.2 Effect of Fatigue Cycling on Other Parameters

Several of the parameters analyzed in Reeve's research were determined for the fatigue run-out specimens and in turn compared to Reeve's results. These parameters, which included ductility, maximum deflection, maximum load, and general yield, did not appear to be significantly affected by the fatigue conditioning considered (see Figures 4-5 through 4-8).

Figure 4-5 shows the observed deflection ductility ratios for all specimens tested. From the data shown, it can be inferred that the cyclic loading had little or no effect ductility of the test specimens studied in this program. The L2F and H4F specimens exhibited greater ductilities than their companion L2 and H4 specimens, while the H2x1F and L4F specimens experienced a decrease in ductility. These small variations in behavior are well within expected scatter for reinforced concrete members and can be attributed to variations in material properties, member dimensions and quality control during construction of the beams and application of the CFRP. The observation that the softer adhesive (L) exhibits marginally improved displacement ductility over the H adhesive (Reeve 2005) continues to be reflected following fatigue conditioning.

Figure 4-6 displays the maximum observed deflections for all specimens. Slight variations in behavior exist, although no effect from fatigue conditioning may be identified

Figure 4-7 displays the maximum capacity of each specimen and Figure 4-8 shows the capacity as general yield. Figures 3-2, 3-4, 3-7, 3-8 and Figures 4-7 and 4-8 show that the load carrying capacity of each fatigue conditioned beam was not affected by the cyclic loading. As noted by Reeve, the incremental improvement in capacity diminishes with increasing CFRP material used.

Table 4-1 Measures of fatigue behavior

	ratio of final (N_f) to initial (N = 2) stress range	average rate of change of stress range with cycling	ratio of final (N_f) to initial (N = 2) secant stiffness	average rate of change of stiffness with cycling
		ksi/100k cycles		kip/in/100k cycles
L1F	0.93	-0.62	0.93	-0.14
L2F	1.16	0.24	0.82	-0.08
L2x1F	1.11	0.73	0.92	-0.15
L4F	1.15	0.19	0.82	-0.10
H1F	1.04	0.36	0.92	-0.15
H2F	1.09	0.23	0.94	-0.05
H2x1F	1.14	0.22	0.82	-0.08
H4	1.12	0.15	0.88	-0.06

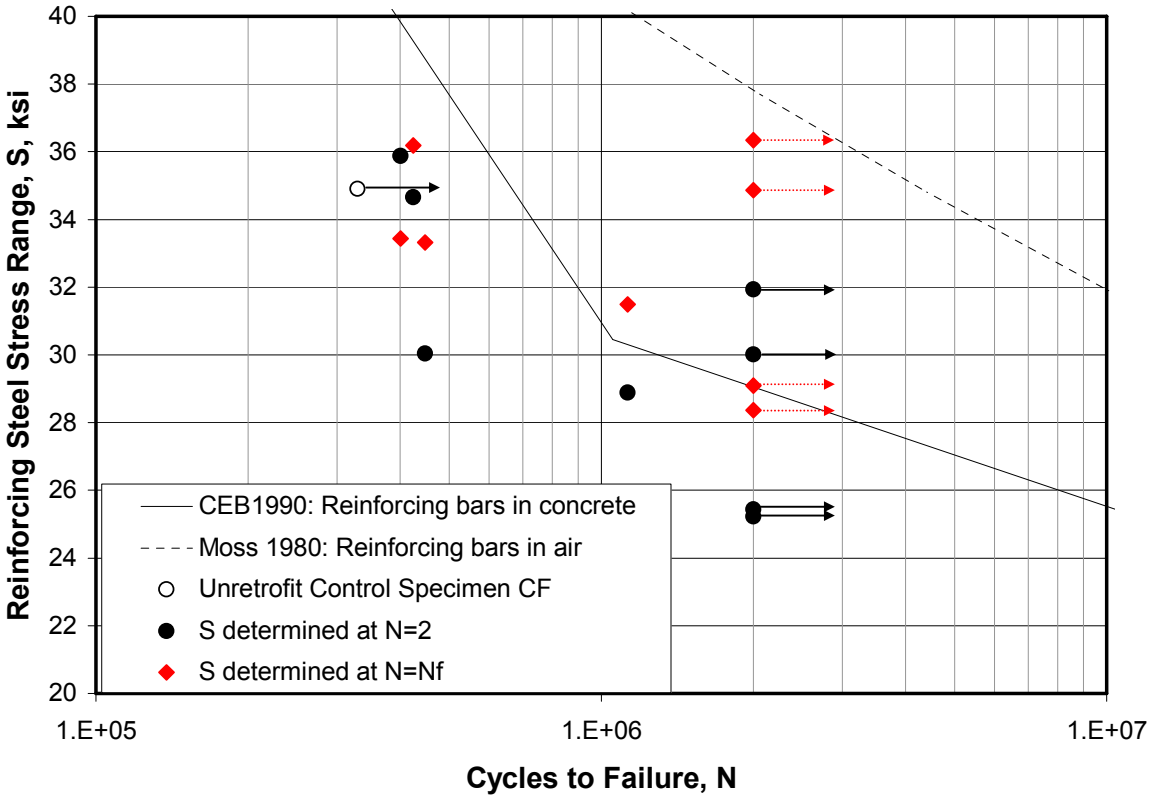

Figure 4-1 S-N data determined at N = 2 and N=N_f.

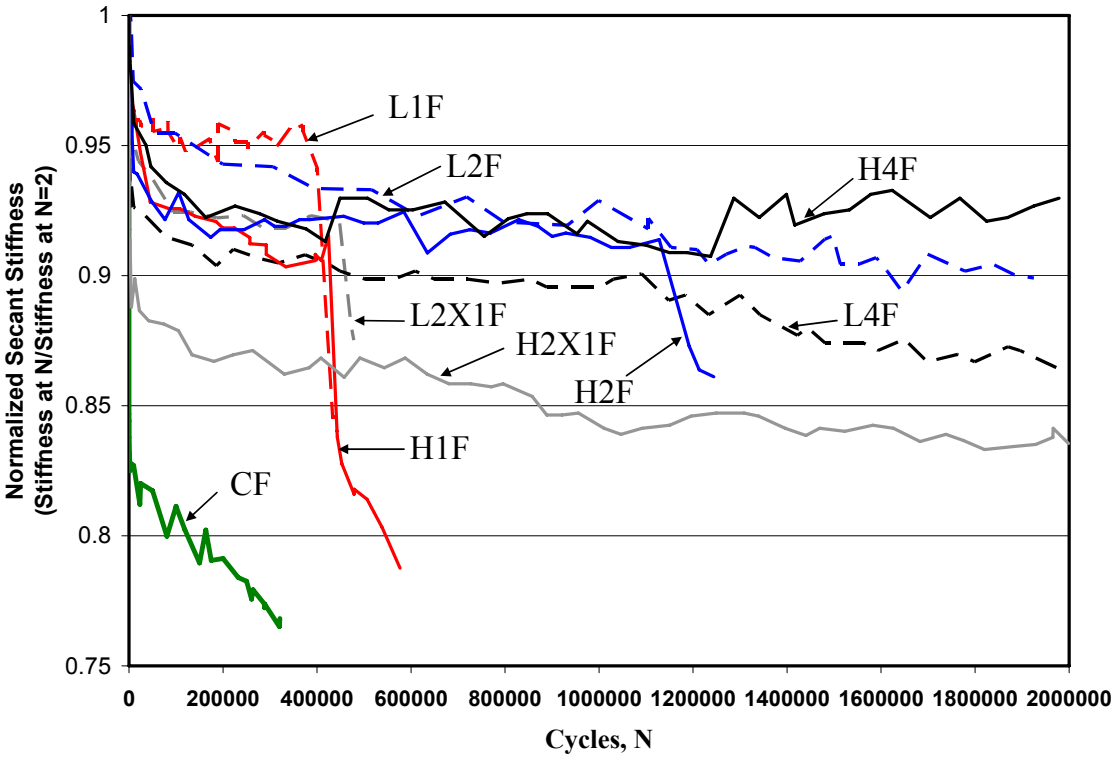

Figure 4-2 Stiffness degradation with fatigue cycling.

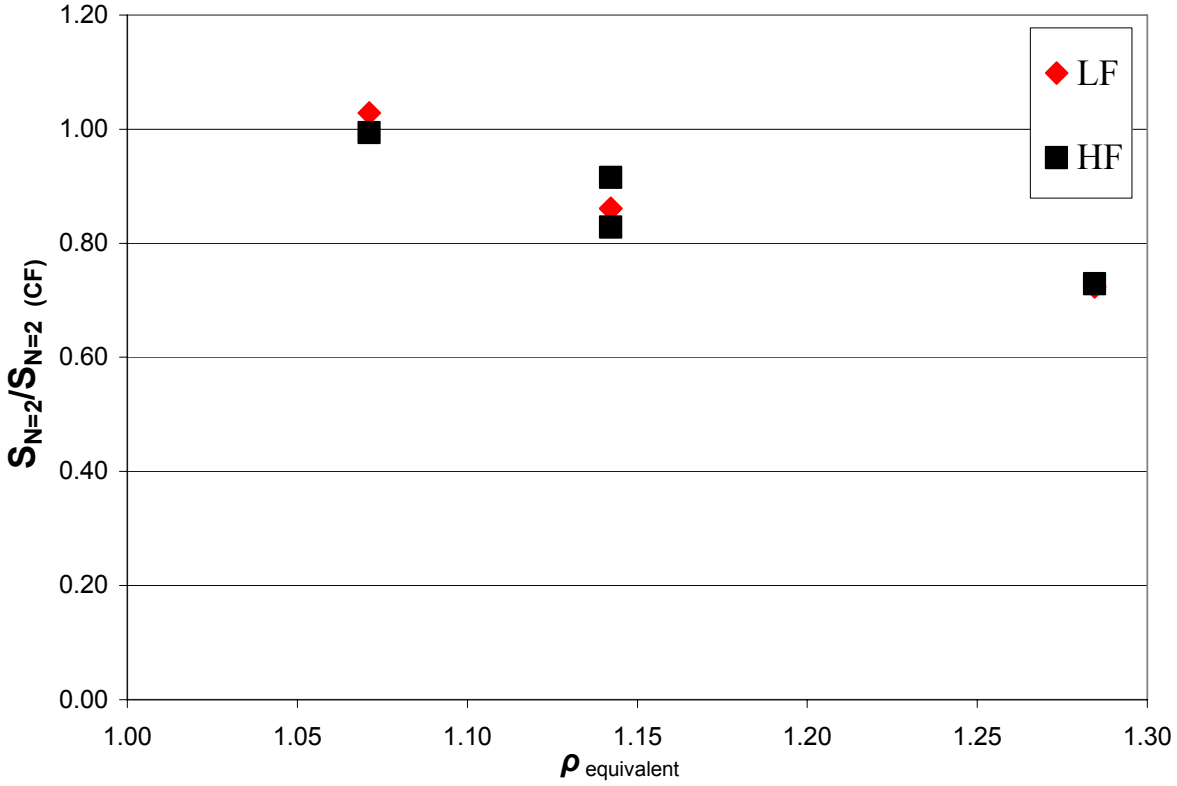

Figure 4-3 Effect of amount of CFRP on fatigue stress range at N = 2.

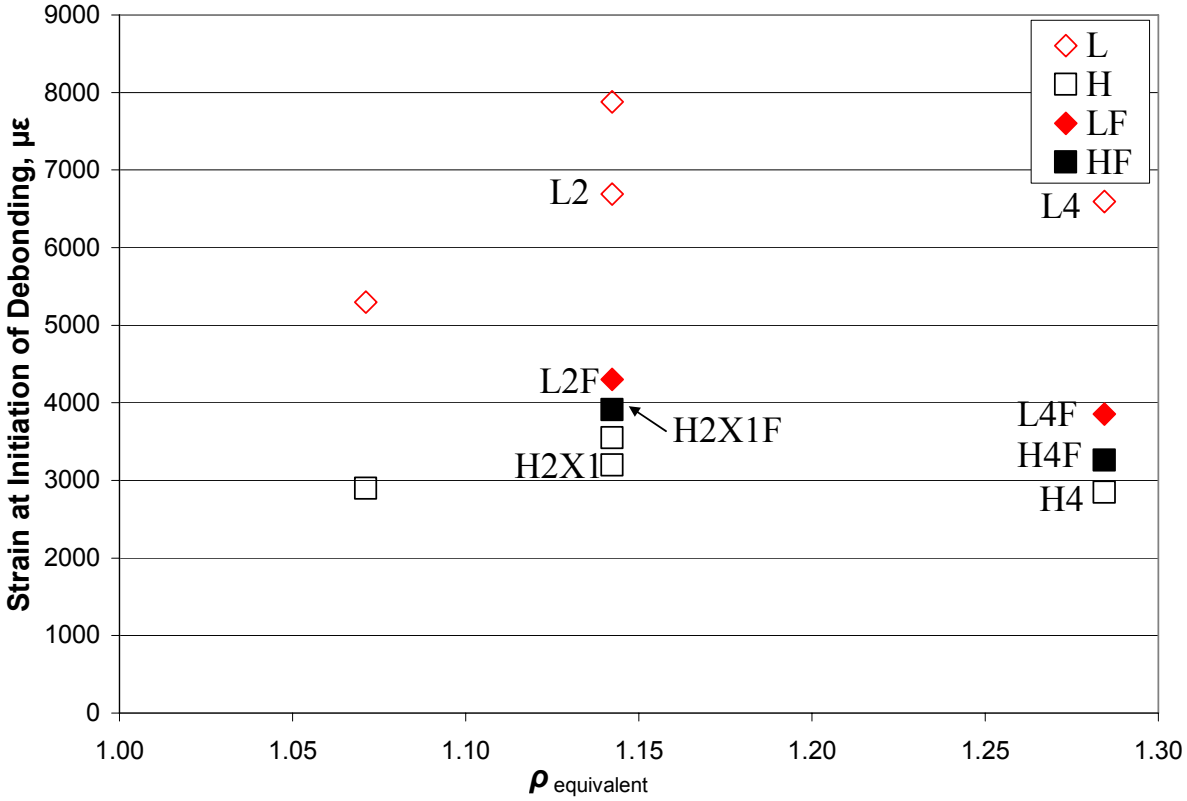

Figure 4-4 Effect of amount of CFRP on CFRP strain at initiation of debonding.

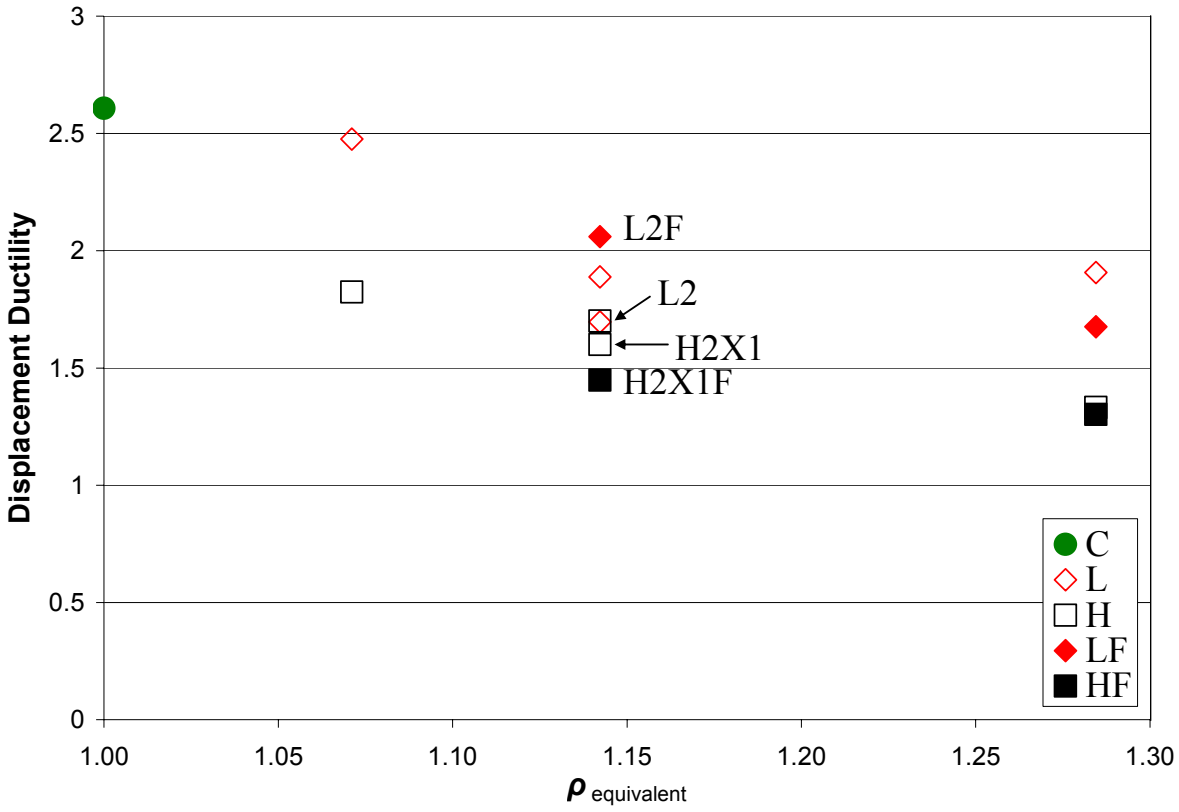

Figure 4-5 Effect of amount of CFRP on displacement ductility.

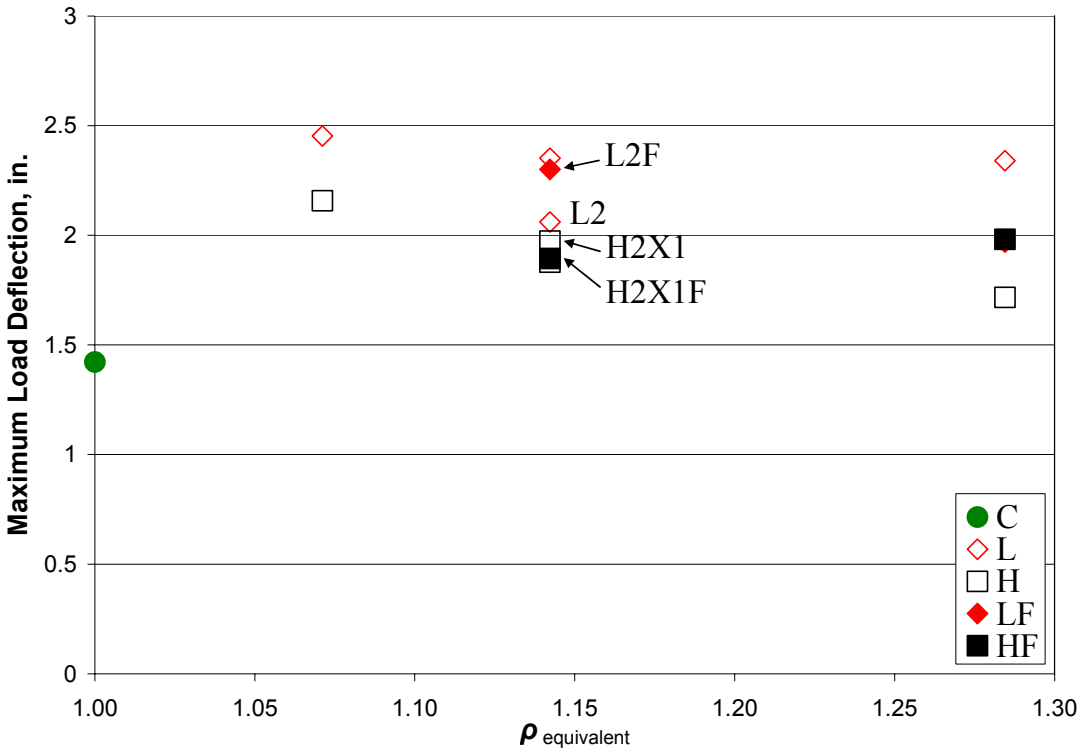

Figure 4-6 Effect of amount of CFRP on deflection at maximum load.

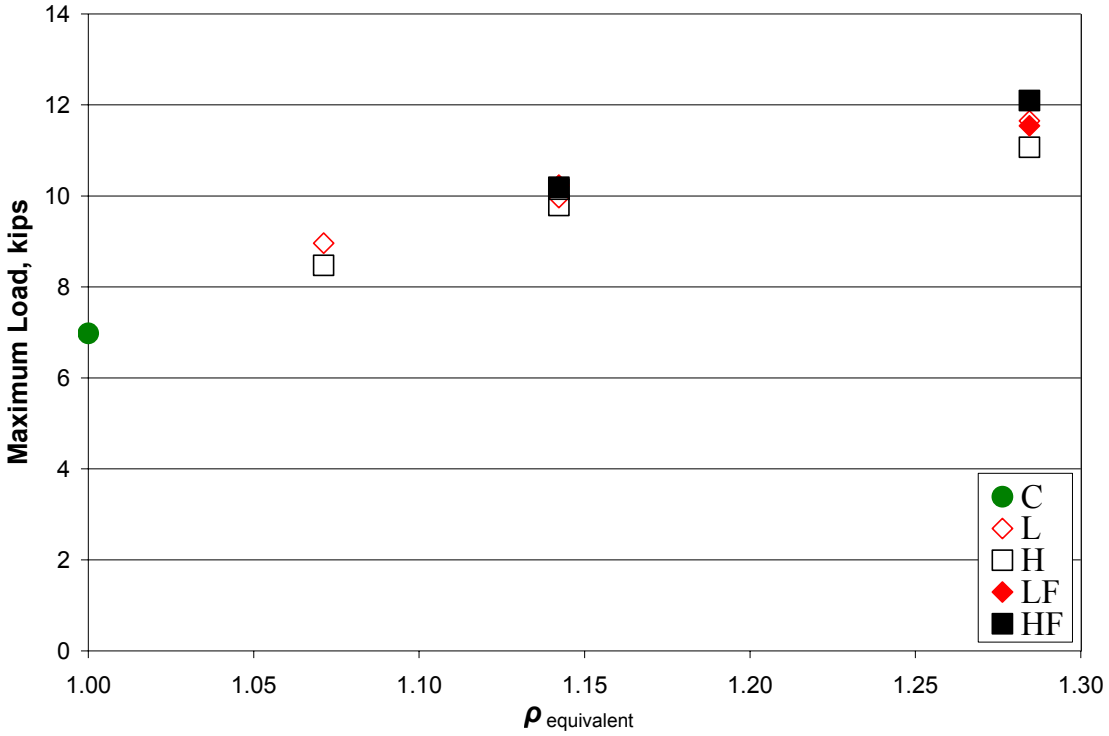

Figure 4-7 Effect of amount of CFRP on maximum load.

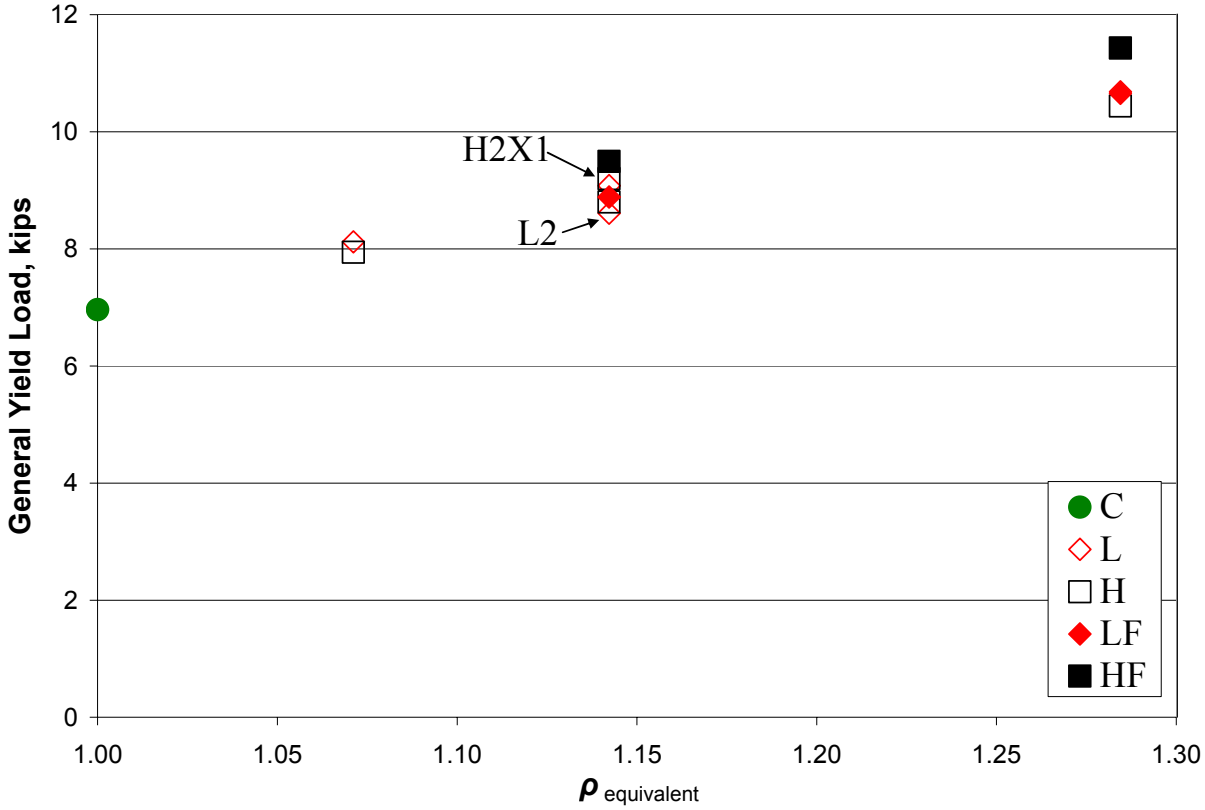

Figure 4-8 Effect of amount of CFRP on general yield load.

5.0 SUMMARY, CONCLUSIONS, AND RECOMMENDATIONS

This chapter reports and discusses conclusions of the experimental program. A summary of the test procedure and continuing needs/areas for future work are also presented.

5.1 SUMMARY OF TEST PROGRAM

Nine test specimens were tested under fatigue loading conditions. Each specimen measured 10" (254 mm) deep by 6" (152 mm) wide. Eight of the specimens were retrofitted with carbon fiber reinforced polymer (CFRP) and one specimen was left unretrofit and used as the control fatigue specimen. All beams had three #4 longitudinal reinforcing bars as primary flexural reinforcement, resulting in a steel reinforcement ratio of 1.0%.

The CFRP material used was a commercially available product. The material came in strips that measured 4" (102 mm) wide by 0.055" (1.4 mm) thick. The CFRP material was applied to the soffits of the beams using the conventional adhesive applied (CAA) method. Four different CFRP configurations and two different adhesives were used. The adhesives were also commercially available products. One adhesive was a "high-modulus" adhesive and the other was a "low-modulus" adhesive. The low-modulus adhesive was approximately half as stiff as the high-modulus adhesive.

In order to investigate the effect of CFRP strip geometry and configuration on the fatigue life of a specimen, four different CFRP configurations were used. All configurations were extended to within a few inches of the supports. Each arrangement was installed using both the low-modulus adhesive and the high-modulus adhesive. The 4" (102 mm) wide strip was cut into 1" (25mm), 2" (51mm), and 4" (102 mm) widths. The first configuration consisted of a single 1"

(25 mm) strip applied down the center line of the beam. The second configuration consisted of a single 2" (51 mm) strip applied down the center line of the beam. The third configuration consisted of two 1" (25 mm) strips spaced 2" (51 mm) apart and applied down the center line of the beam. The last configuration was a single 4" (102 mm) strip applied down the centerline of the beam.

All nine specimens were tested under mid-point cyclic loading until failure or 2,000,000 cycles. The beams were supported over a clear span of 178 5/8" (4537 mm). The #4 reinforcing bar of each beam was instrumented with 4 electrical resistance strain gages spaced 12" (305 mm). The CFRP was also instrumented with 4 electrical resistance strain gages located at the locations of the corresponding reinforcing bar strain gages. The mid-span displacement and the applied load were recorded in addition to the corresponding reinforcing bar and CFRP strains. The cyclic loading pattern used was a sinusoidal wave with a maximum frequency of 1.7Hz. The load ranged from 1 kip (4.45 kN) to 5 kips (22.24 kN) for all specimens. If a specimen sustained 2,000,000 cycles of loading, the fatigue test was terminated and a monotonic test to failure commenced. Unlike the fatigue tests, the monotonic test to failure was done in stroke control at a rate of deflection of the beam of 0.13" (3.4 mm) per minute.

5.2 CONCLUSIONS

All specimens (L1F, L2x1F, H1F and H2F) that failed during the fatigue cycling (i.e.: N_f < 2,000,000) failed through fatigue-induced rupture of the internal reinforcing steel. All specimens (L2F, L4F, H2x1F, and H4F) which were monotonic run-out specimens (i.e.: N_f = 2,000,000) exhibited intermediate crack induced debonding behavior. Debonding was the primary mode of failure for all monotonic run-out specimens. The following conclusions have been drawn from this work:

1. The observed S-N behavior is relatively "flat" indicating that the stress range in the reinforcing steel is close to the expected endurance limit for the reinforcing bar material. Thus, the final behavior is highly sensitive to the behavior of bonded CFRP systems.
2. Stress range drift must be considered when designing a bonded retrofit that is to perform in fatigue. Stress ranges in the primary steel reinforcement were noted to increase (at $N = N_f$) from 4% to 16% from the initial stress range calculated at cycle N=2. The increase in stress range is proportional to the number of fatigue cycles the beam undergoes.
3. The secant stiffness of a section generally degrades at a rate proportional to the fatigue life of the beam. Degradation is essentially the same for all retrofit configurations and adhesive types. This indicates a sound bond during fatigue cycling in all cases considered.
4. In general, the stress range in the internal reinforcing steel decreases as the amount of CFRP increases. As the b_f/b ratio or equivalent reinforcement ratio increases, S decreases. This relationship appears to be linear at the fatigue (service) load levels considered. At ultimate conditions the incremental increase in capacity is reduced with an increasing amount of CFRP.
5. The stress range reduction resulting from the application of the CFRP results in an increased fatigue life for the specimens considered.
6. The data from the fatigue tests presented are generally within the expected scatter of fatigue data and fit nicely with the existing bonded retrofit database presented in Table 1-1.

7. Contrary to intuition, for these tests, the lower modulus adhesive performance degrades more than that of the higher modulus adhesive when subject to cyclic loading.
8. In general, fatigue cycling of the low-modulus specimens had detrimental effects on the debonding behavior. Debonding strains in the run-out LF specimens were seen to decrease significantly when compared to the debonding strains of their companion L specimens reported by Reeve (2005). This effect was not seen in the HF and H specimens. This indicated that that the nature of the adhesive should be included when calculating the expected debonding strain under fatigue loads.
9. In general, the fatigue conditioning had only a marginal effect on other response parameters such as ductility, ultimate capacity, maximum deflection, and general yield load of the beams.

5.3 RECOMMENDATIONS

This test program is one of few conducted in the area of the fatigue behavior of reinforced concrete beams retrofitted with FRP. Further research efforts are essential to propagating the use of FRP material for retrofitting, particularly in potentially fatigue-sensitive applications such as bridge decks. Some recommendations for future study include:

1. There is certainly an effect of fatigue on FRP retrofits. This effect is affected by adhesive properties. Future research needs to focus more on adhesive properties to fully quantify their role in the behavior of these types of retrofits.
2. The stress ranges of the experiments presented in this work were around the endurance limit for the reinforcing steel. Future work needs to focus on higher stress ranges to better characterize the S-N relationship and to establish the role of bond in

fatigue behavior. It is possible that the common wisdom that fatigue behavior is controlled by the stress in the reinforcing steel has it limits.

3. Future research needs to focus on low stress ranges also. The LF run-out specimens from the test regimen presented here exhibited interesting debonding behavior in that the debonding strains were considerably less than if they had not been fatigue conditioned. A new test regimen involving different adhesives and a relatively low stress range fatigue conditioning program followed by a monotonic push to failure would allow a much more complete study of what was revealed through the run-out specimens of this work.

It is evident that the behavior of the FRP is very difficult to characterize. Extensive further studies will be necessary to fully understand debonding FRP. The mechanism behind debonding is easily understood, but trying to pinpoint the exact moment in time, location and strain at which it occurs is another feat. Additionally, it is believed that the propagation (both load-induced and creep-induced) of debonding affects behavior. It is recommended that improved methods be developed to detect debonding. A pilot application of such a novel debond detection scheme was applied to Specimen L4F in the present study and is reported elsewhere (Kim et al., 2006).

APPENDIX

KEY RESULTS FROM REEVE 2005

Table A-1 Summary of Key Results from Reeve (2005)

		C	L1	L2	L2X1	L4	H1	H2	H2X1	H4
b_f/b		0	0.17	0.33	0.33	0.67	0.17	0.33	0.33	0.67
adhesive type		na	SikaDur 23				SikaDur 30			
age at start of test	days	144	154	157	161	228	162	163	165	170
cracking load	kips	<0.66	0.62	0.66	0.63	0.75	0.55	0.64	0.64	0.65
cracking moment	kip-in	<30	28	29	28	33	25	29	29	29
load at initial yield of reinforcing	kips	5.91	6.05	6.78	5.99	7.31	6.16	6.38	6.63	8.44
moment at initial yield of reinforcing	kip-in	264	270	303	267	326	275	285	296	377
deflection at initial yield of reinforcing	in	0.98	1.07	1.00	0.84	1.46	0.98	0.95	0.89	1.08
load at general yield	kips	6.96	8.12	8.61	9.08	10.68	7.94	8.80	9.20	10.44
moment at general yield	kip-in	311	363	384	405	477	355	393	411	466
deflection at general yield	in	1.18	1.35	1.32	1.35	1.49	1.32	1.36	1.30	1.40
maximum load	kips	6.98	8.96	9.96	10.23	11.65	8.47	9.79	10.15	11.07
maximum moment	kip-in	312	400	445	457	520	378	437	453	494
deflection at max load	in	1.42	2.45	2.06	2.35	2.34	2.16	1.88	1.97	1.72
deflection at ultimate load (80% max)	in	3.08	3.34	2.24	2.55	2.84	2.41	2.18	2.21	1.86
displacement ductility		2.61	2.48	1.70	1.89	1.91	1.82	1.60	1.70	1.33
maximum observed strain in FRP	με	na	8370	6688	7878	6595	6466	6200	6863	4813
corresponding rebar strain	με	15932	n.r.	13167	6620	15337	12414	14812	6004	9952
maximum strain in FRP at time of max load	με	na	8218	6518	7872	6462	6160	6112	6853	4787
corresponding rebar strain	με	2759	11559	13124	6624	14422	12446	14663	6034	9947
strain in FRP at initiation of debonding	με	na	5300	6688	7878	4540	2900	3550	3200	2850
corresponding rebar strain	με	na	2600	n.r.	n.r.	2990	2300	2680	2790	2500

REFERENCES

Agarwal, B.D. and L.J. Broutman (1990) Analysis and Performance of Fiber Composites, Wiley-Interscience, Hoboken, NJ.

Aidoo, J. (2004) *Flexural Retrofit of Reinforced Concrete Bridge Girders Using Three CFRP Systems*, Ph.D. Dissertation, Department of Civil and Environmental Engineering, University of South Carolina, 197 pp.

Aidoo, J., Harries, K.A. and Petrou, M.F. (2006) "Full-scale Experimental Investigation of Repair of Reinforced Concrete Interstate Bridge using CFRP Materials", *Journal of Bridge Engineering*. Vol. 11, No. 3 (in press)

American Concrete Institute (ACI) Committee 440 (2002) *ACI 440.2R-02 Guide for the Design and Construction of Externally Bonded FRP Systems for Strengthening Concrete Structures*. 45 pp.

American Concrete Institute (ACI) Committee 440 Task Group on Bond of Externally Bonded FRP (2006) *Current Recommendations and Guidelines for Mitigating Debonding Failures in Adhesively Bonded, Externally Applied FRP Applications.* (K. Harries, chair) Committee Report.

Barnes, R.A. and G.C. Mays (1999) "Fatigue Performance of Concrete Beams Strengthened with CFRP Plates", *Journal of Composites for Construction*, Vol. 3, No. 2. pp63-72.

Breña, S.F., Wood, S.L. and Kreger, M.L. (2002) "Fatigue Tests of Reinforced Concrete Beams Strengthened using Carbon Fiber Reinforced Polymer Composites", *Proceedings of the Second International Conference on Durability of Fibre Reinforced Polymer (FRP) Composites for Construction*, Sherbrooke, Canada, pp575-586.

Comité Euro-International du Beton (1990) CEB/FIB *Model Code 1990*. Thomas Telford, London. 437pp.

Concrete Society (2004) *Design Guidance for Strengthening Concrete Structures Using Fibre Composite Materials* Technical Report 55. Camberly, UK.

Curtis, P.T. (1989) "The Fatigue Behaviour of Fibrous Composite Materials." *Journal of Strain Analysis*, Vol. 24, No. 4. pp235-244.

Deskovic, N., U. Meier, et al. (1995) "Innovative Design of FRP Combined with Concrete: Long-Term Behavior", *Journal of Structural Engineering*, Vol. 121, No. 7., pp1079-1089.

El-Tawil, S., C. Ogunc, et al. (2001) "Static and Fatigue Analyses of RC Beams Strengthened with CFRP Laminates", *Journal of Composites for Construction*, Vol. 5, No. 4. pp258-267.

Federation Internationale du Beton (CEB) (2001) *fib Bulletin 14: Externally Bonded FRP Reinforcement for RC Structures*.

Fyfe Company LLC, (2005) Technical Product Data Sheet
http://www.fyfeco.com/products/misc.html, accessed December 1, 2005.

Gussenhoven, R. and Breña, S.F. (2005) SP-230-36: "Fatigue Behavior of Reinforced Concrete Beams Strengthened with Different FRP Laminate Configurations", *International Symposium on Fiber Reinforced Polymer (FRP) Reinforcement for Concrete Structures*, Kansas City, Missouri, University of Minnesota, 2005.

Hahn, H.T. (1979) "Fatigue Behavior and Life Prediction of Composite Laminates" *ASTM STP 674*, pp383-417.

Harries, K.A. and J. Aidoo (2005) "Deterioration of FRP-to-Concrete Bond Under Fatigue Loading." *International Symposium on Bond Behaviour of FRP in Structures*, Hong Kong, International Institute for FRP in Construction, 2005.

Harries, K. A. (2005) "Fatigue Behaviour of Bonded FRP Used for Flexural Retrofit." *International Symposium on Bond Behaviour of FRP in Structures*, Hong Kong, International Institute for FRP in Construction, 2005.

Heffernan, P.J. (1997) *Fatigue Behaviour of Reinforced Concrete Beams Strengthened with CFRP Laminates*, Ph.D. Dissertation, Department of Civil Engineering, Royal Military College of Canada, Kingston, Ontario.

Helgason, T. and Hanson, J.M. (1974) "Investigation of Design Factors Affecting Strength of Reinforcing Bars-Statistical Analysis", *Abeles Symposium on Fatigue of Concrete*, SP-41 ACI, pp107-138.

International Concrete Repair Institute (1997) *Concrete Surface Profile Chips*. ICRI, Sterling, VA.

Japan Society of Civil Engineers (JSCE) (2001) *Recommendations for the Upgrading of Concrete Structures with use of Continuous Fiber Sheets*. Concrete Engineering Series 41, 250 pp. (available in English on CD)

Kim, S.D., In, C.W., Cronin, K., Sohn, H, and Harries, K.A. (2006) "Active Sensing for Disbond Detection in FRP Strengthened RC Beams" *Proceedings of the 24th International Modal Analysis Conference (IMAC)*, St. Louis, Jan-Feb 2006.

Kotynia, R. and Kaminska, M.E. (2003) *Ductility and failure mode of RC beams strengthened for flexure with CFRP*, Report No. 13. Department of Concrete Structures, Technical University of Lodz. 51 pp.

Maeda, T., Komaki, H., Tsubouchi, K., Murakami, K. (2002) "Strengthening Effect of Carbon Fiber Sheet Adhesion Method Using Flexible Layer", *Transactions of the Japan Concrete Institute*, Vol.23, pp185-192.

Mallet, G. (1991) *Fatigue of Reinforced Concrete*. Transportation and Road Research Laboratory (TRRL) State of the Art Review / 2, London, U.K.

Mandell, J.F. (1982) "Fatigue Behaviour of Fiber Resin Composites", *Developments in Reinforced Plastics*, Vol. 2, pp67-107.

Masoud, S., Soudki, K. and Topper, T. (2001) "CFRP-Strengthened and Corroded RC Beams under Monotonic and Fatigue Loads", *Journal of Composites for Construction*, Vol. 5, No. 4., pp228-236.

Meier, U., Deuring, M., Meier, H. and Schwegler, G. (1993) "Strengthening of Structures with Advanced Composites" *Alternate Materials for the Reinforcement and Prestressing of Concrete*, J.L. Clarke, editor, Blackie Academic and Professional, Glasgow.

Minnaugh, P. (2006) *Experimental Behavior of Steel Reinforced Polymer Retrofit Measures*. MS Thesis, University of Pittsburgh Department of Civil and Environmental Engineering, May 2006.

Moss, D.S. (1980) "Axial Fatigue of High Yield Reinforcing Bars in Air", Transport and Road Research Laboratory *Report SR622*.

National Research Council (1991) "Life Prediction Methodologies for Composite Materials", *Committee on Life Prediction Methodologies for Composites – NMAB 460*, National Materials Advisory Board, Washington DC, 66pp.

National Research Council (CNR) (2004) "Guidelines for Design, Execution and Control of Strengthening Interventions by Means of Fibre-reinforced Composites", *Advisory Committee on Technical Regulations for Construction*, Rome, Italy, National Research Council, 204pp.

Papakonstantinou, C.G., Petrou M.F. and Harries, K.A. (2001) "Fatigue of Reinforced Concrete Beams Strengthened with GFRP Sheets", *Journal of Composites for Construction*, Vol. 5, No. 4., pp246-253.

Quattlebaum, J.B., (2003) *Comparison of Three CFRP Flexural Retrofit Systems under Monotonic and Fatigue Loads*, MS Thesis, Department of Civil and Environmental Engineering, University of South Carolina, Columbia, SC.

Quattlebaum, J., Harries, K.A. and Petrou, M.F., (2005) "Comparison of Three CFRP Flexural Retrofit Systems Under Monotonic and Fatigue Loads.", *ASCE Journal of Bridge Engineering*. Vol. 10, No. 6 pp731-740.

Reeve, B.Z., (2005) *Effect of Adhesive Stiffness and CFRP Geometry on the Behavior of Externally Bonded CFRP Retrofit Measures Subject to Monotonic Loads*, *MS Thesis,* Department of Civil and Environmental Engineering*,* University of Pittsburgh, December 2005.

Roylance, M. and Roylance, O. (1981) "Effect of Moisture on the Fatigue Resistance of Aramid-Epoxy Composite", *Organic Coatings and Plastics Chemistry*, Vol. 45, pp784-788.

Sebastian, W.M. (2001. "Significance of Midspan Debonding Failure in FRP-Plated Concrete Beams", *Journal of Structural Engineering* Vol. 125, No. 7., pp792-798.

Shahawy, M. and T.E. Beitelman (1999) "Static and Fatigue Performance of RC Beams Strengthened with CFRP Laminates." *Journal of Structural Engineering* Vol. 125, No. 6., pp613-621.

Sika Corporation (2005) Technical Product Data Sheet, http://www.sikaconstruction.com/con/con-prod-name.htm#con-prod-Sikadur23LoModGel, accessed December 1, 2005.

Tilly, G.P. and Moss, D.S. (1982) "Long Endurance Fatigue of Steel Reinforcement", *IABSE Reports, International Association for Bridge and Structural Engineering*, 37, Zurich, Switzerland, pp229-238.

Teng, J.G., Smith, S.T., Yao, J. and Chen, J.F. (2001) "Intermediate Crack Induced Debonding in RC Beams and Slabs", *Construction and Building Materials*, Vol. 17, No. 6-7, pp 447-462.

Teng, J.G., Lu, X.Z., Ye, L.P. and Jiang, J.J. (2004) "Recent Research on Intermediate Crack Induced Debonding in FRP Strengthened Beams." *Proceedings of the 4th International Conference on Advanced Composite Materials for Bridges and Structures*, Calgary 2004.